Semi-Intrusive Stochastic Galerkin Finite Element Method for Adjoint-Based Optimization Under Uncertainty

Komahan Boopathy * and Graeme J. Kennedy†
Georgia Institute of Technology, Atlanta, GA, 30332

The stochastic Galerkin method for the propagation of probabilistically modeled uncertainties can be difficult to apply in practice due to its formulation and the challenge of creating a computational infrastructure to support it. To address these challenges, this work proposes a sampling-based stochastic Galerkin method that leverages existing deterministic analysis and adjoint-based derivative implementations. The proposed formulation is semi-intrusive, since it is implemented using an existing deterministic framework, requiring only the numerical sampling of the deterministic residuals, Jacobians, boundary conditions, and adjoint implementations at nodes in the probabilistic domain. The software architectures to support stochastic generalizations of the deterministic finite element frameworks are presented. This proposed approach is demonstrated on a finite-element framework for flexible multibody dynamics problems. Finally, the semi-intrusive implementation of the stochastic Galerkin method is used to demonstrate adjoint gradient-based optimizations of flexible multibody dynamics systems in the presence of probabilistically modeled uncertainties.

Nomenclature

$\boldsymbol{x}, \mathcal{D}$	=	design variables and design domain
$t, \mathcal{T}$	=	temporal variable and time domain
t_0, t_f	=	initial and final time
$\boldsymbol{u}(\boldsymbol{x}, t)$	=	deterministic state variables
$\boldsymbol{R}(\boldsymbol{x}, t; \boldsymbol{u}(\boldsymbol{x}, t))$	=	residuals of the deterministic differential equations
$F(\boldsymbol{x}, t; \boldsymbol{u}(\boldsymbol{x}, t))$	=	spatio-temporal output function for performance evaluation
$\bar{F}(\boldsymbol{x})$	=	spatio-temporal average or extrema of the output
$\boldsymbol{y}, \mathcal{Y}$	=	probabilistic random variable (aleatory) and probabilistic random domain
M	=	number of the probabilistic random variables
$\rho(\boldsymbol{y})$	=	probability density function

*School of Aerospace Engineering, 270 Ferst Drive, komahan@gatech.edu, AIAA Member.
†School of Aerospace Engineering, 270 Ferst Drive, graeme.kennedy@aerospace.gatech.edu, AIAA Associate Fellow.

$\mathcal{N}$	=	normal probability distribution
$\mathcal{U}$	=	uniform probability distribution
$\mathcal{E}$	=	exponential probability distribution
N	=	number of orthonormal basis functions
$\psi_n(\boldsymbol{y})$	=	$n-$th orthonormal basis function
P	=	number of deterministic degrees of freedom in the finite element model
Q	=	number of quadrature points from the probabilistic domain
$\boldsymbol{y}_q = [y_1^q, y_2^q, \ldots, y_M^q]$	=	$q-$th quadrature node/point from the probabilistic domain
α_q	=	corresponding weight of the $q-$th quadrature node from the probabilistic domain
$\mathbf{u}(\boldsymbol{x}, t, \boldsymbol{y})$	=	stochastic state variables
$\mathbf{R}(\boldsymbol{x}, t, \boldsymbol{y}; \mathbf{u}(\boldsymbol{x}, t, \boldsymbol{y}))$	=	residuals of the stochastic differential equations
$\mathsf{F}(\boldsymbol{x}, t, \boldsymbol{y}; \mathbf{u}(\boldsymbol{x}, t, \boldsymbol{y}))$	=	probabilistic-spatio-temporal output
$\bar{\mathsf{F}}(\boldsymbol{x}, \boldsymbol{y})$	=	spatio-temporal average or extrema of the probabilistic-spatio-temporal output
$\mathbb{E}[\cdot], \mathbb{V}[\cdot], \mathbb{S}[\cdot]$	=	expectation, variance, and standard deviation operators
$\mathbf{v}(\boldsymbol{x}, t, \boldsymbol{y}), \mathbf{w}(\boldsymbol{x}, t, \boldsymbol{y})$	=	stochastic adjoint state variables for $\mathbb{E}[\mathsf{F}]$ and $\mathbb{E}[\mathsf{F}^2]$, respectively
$f(\boldsymbol{x})$	=	optimization objective function
$\boldsymbol{c}(\boldsymbol{x})$	=	optimization inequality constraint functions

I. Introduction

The goal of optimization under uncertainty (OUU) is to enable the systematic incorporation of uncertainties into design optimization problems [1–10]. To apply OUU to relevant aerospace applications, there is a need to create computational infrastructure that applies uncertainty quantification (UQ) to high-fidelity simulations such as flexible multibody dynamics. Figure 1 illustrates the key elements required for gradient-based OUU: (1) evaluations of output functions from simulations governed by partial differential equations (PDEs), (2) the evaluation of statistics of the PDE outputs, and (3) the evaluation of the derivatives of the statistics for optimization. However, the development effort needed to implement both uncertainty propagation techniques and adjoint-based derivative evaluation methods is a significant impediment to the broader adoption of OUU. To address this issue, we propose a semi-intrusive approach that enables the extension of an adjoint-enabled deterministic finite-element framework to OUU problems. The proposed method is semi-intrusive since it leverages the original deterministic implementation to create a stochastic finite-element framework.

Methods for uncertainty analysis can be categorized as either stochastic sampling methods (SSMs) [11–18] or stochastic projection methods (SPMs) [16, 19–32]. The SPMs are categorized further as either stochastic spectral

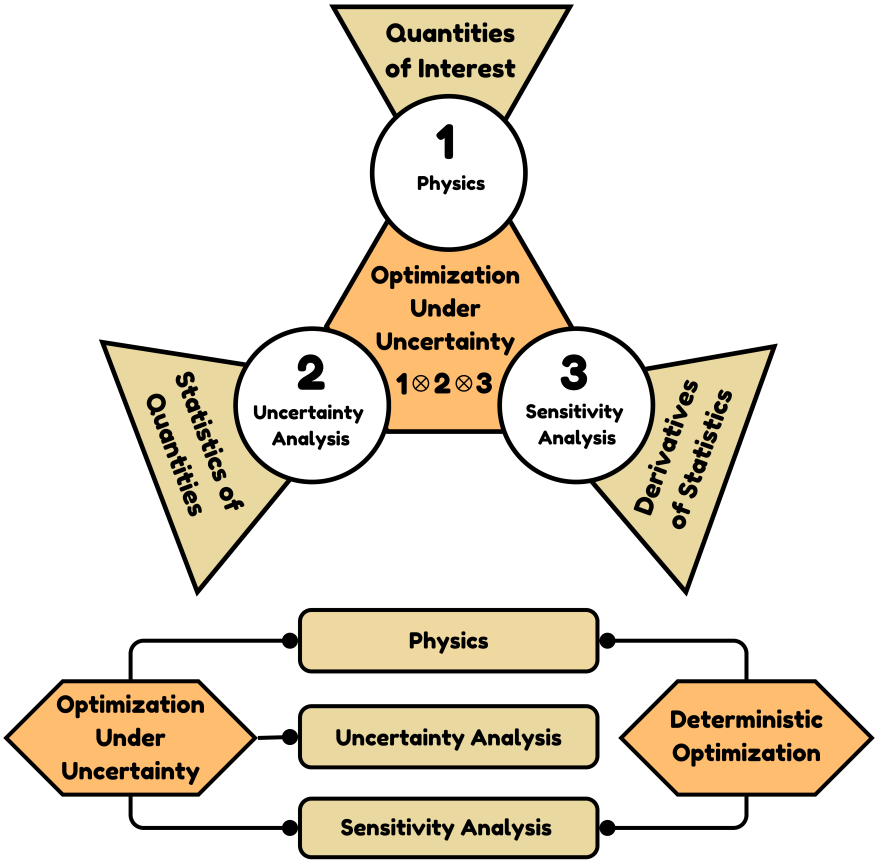

Fig. 1 A schematic of the analysis categories spanning optimization under uncertainty and deterministic optimization.

projection (SSP) methods [19, 20] or stochastic Galerkin-projection methods (SGMs) [16, 21–34]. The SSM and SSP are non-intrusive, whereas the SGM is intrusive, requiring end-to-end source code implementations for applications. The simplicity, accuracy, robustness, scalability, and efficiency of uncertainty propagation methods through the existing physics and adjoint simulation frameworks are crucial in the context of multidisciplinary analysis and optimization. Towards the vision of solving large-scale OUU problems [9], this investigation focuses on addressing key issues related to the application of SGM through existing physics and adjoint sensitivity analysis frameworks

The propagation of uncertainties using the SSM is based on multiple solutions of the deterministic PDEs for the sampling nodes selected from the probabilistic domain $\mathcal{Y}$. The sampling nodes are chosen based on deterministic quadrature schemes from probability distributions, as random realizations from probability distributions, as partially random Latin hypercube samples, or as fully random Monte Carlo samples [10]. The steps involved in SSM are outlined schematically in Figure 2. The SSMs treat the deterministic PDE solution procedure as a black-box operation. The simplicity of SSM makes it a natural choice for UQ and OUU applications. However, SSM implementations may suffer from a lack of scalability, sacrifice derivative accuracy, and may lack robustness. Each of these issues is described below.

- **Scalability of forward and reverse problems**: The computational cost of solving deterministic PDEs scales

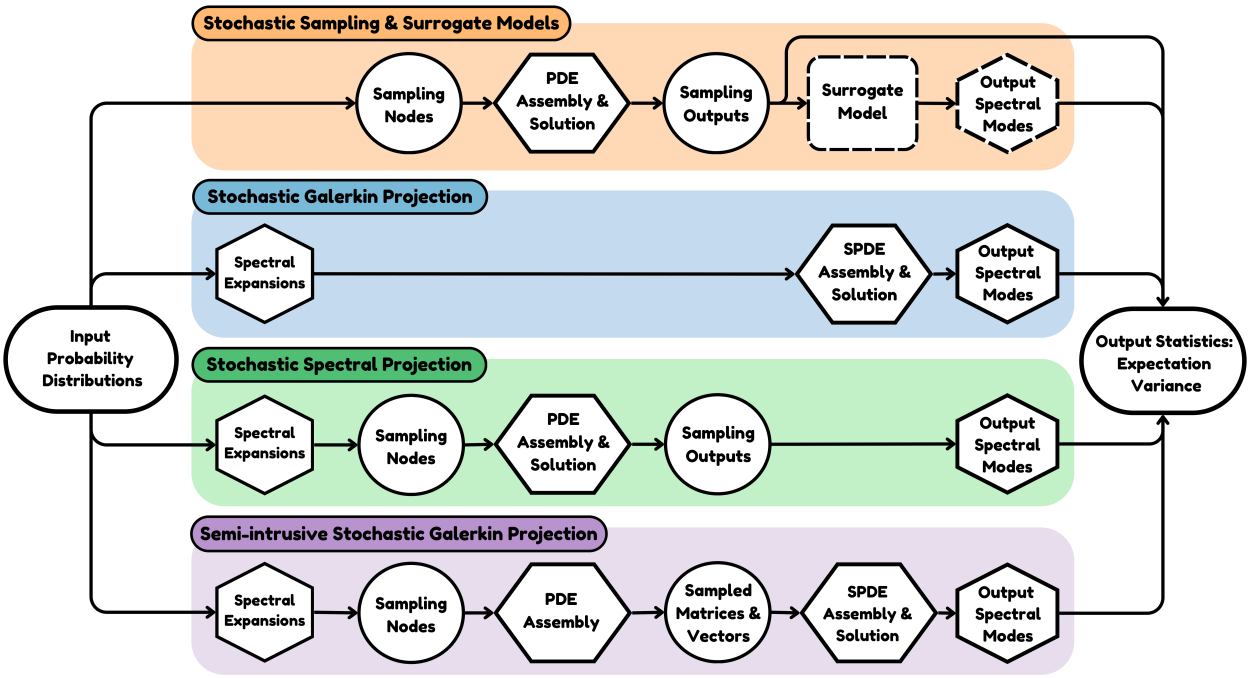

Fig. 2 A schematic representation of combinatorics in the placement of sampling and spectral expansion principles forming different UQ methods. The use of sampling reduces intrusiveness.

linearly with the number of samples, Q, and non-linearly with the number of probabilistic dimensions, M, resulting in the curse of dimensionality. To mitigate this issue, the SSMs employ sparse sampling grids and adaptive sampling instead of full-tensor grids [17, 35] to evaluate output statistics, or construct surrogate-models [36–40] as a proxy for expensive PDE outputs and sample the surrogate model to evaluate output statistics (see Figure 2). The less-expensive surrogate model approach may either use non-spectral models such as kriging [38, 40] or spectral models such as polynomial chaos [36, 37, 39, 41]. The cost of building a surrogate model is a function of the dimensionality and sample-set size, which are recognized as scalability bottlenecks [40]. As with the forward-mode solution of PDEs, the reverse-mode adjoint solution to obtain derivatives is also an inherent computational cost for each chosen sample. The deterministic adjoint derivatives are sampled similarly to obtain the derivative of the statistics [2], but this approach again faces the curse of dimensionality.

- **Accuracy of Derivatives**: In the absence of an adjoint implementation, the approximate derivatives of statistics can be evaluated by using finite-difference or complex-step methods [42] which requires multiple solutions of the governing PDEs. The computational cost of this approach grows rapidly with the number of design variables. Alternatively, the surrogate models built to approximate the output functions in the forward-mode can provide inexpensive derivative estimates [39–41]. Due to the lack of scalable options for obtaining derivatives of statistics, approximations such as the derivative evaluated at the mean of input distributions [39, 41] or at a random sample from the distribution [10] are used as the expectation derivative, and often ignore the contributions of the variance

derivatives.

- **Robustness:** The deterministic PDE solvers are relied upon to yield converged solutions for all probabilistic nodes in the sample set. In applications such as risk evaluation of designs where samples are drawn specifically from the tail ends of the probability distributions, a lack of solver robustness necessitates the omission of unconverged outputs from the accumulation of statistics or derivatives.

These cost, accuracy, and robustness considerations are relevant at each design iterate produced by the optimizer until a converged design is obtained. Any combination of these factors can impede large-scale OUU applications.

The SGM applies spectral expansions in the probabilistic domain and factorizes the stochastic fields (states and outputs) into known orthonormal basis functions and undetermined coefficients. The steps in the method are shown schematically in Figure 2. The decomposition coefficients are evaluated by solving a coupled system of equations simultaneously, requiring the development of a specialized computational infrastructure. The formulation of this coupled system of equations is challenging [16] due to the simultaneous application of probabilistic domain discretization along with spatio-temporal PDE discretizations. We denote

- the *probabilistic discretization* as representing the solution fields as a spectrum of orthonormal polynomials and multi-dimensional integration across the probabilistic domain $\mathcal{Y}$ using a set of probabilistic nodes;
- the *temporal discretization* as the application of methods such as the backward differences and Runge–Kutta to integrate fields along the one-dimensional time domain $\mathcal{T}$ using a set of temporal nodes; and
- the *spatial discretization* as the application of finite element method (FEM) to integrate fields across the three-dimensional spatial domain $\mathcal{S}$ using a set of spatial nodes.

The SGM has not found general purpose adoption for UQ, as each application requires a case-by-case formulation and implementation based on the governing stochastic PDEs (SPDEs) and the characterization of input uncertainties [16]. For example, the SGM has been formulated for temporal decay [16], diffusion [16], the Navier–Stokes equations [43], and porous media applications [23]. In contrast to the SSM, the SGM solves a larger system of equations once and does not possess multiple single-point failures, which can be a robustness advantage. However, the scalability of the method is constrained by the larger system of equations. There is considerable interest on the SGM solver scalability aspects like adaptive basis selection [44], algebraic multigrid with preconditioners [45–47] and domain-decomposition [48, 49]. The stochastic Galerkin adjoint method for obtaining derivatives of the statistics is an essential component for scalable OUU applications (see Figure 1), but it has not been reported in the literature.

Another UQ approach that combines both the *sampling* and *spectral expansion* principles for the SPDE solution is the SSP method. In this non-intrusive method, the decomposition coefficients for the spectral basis functions are obtained by sampling the output of the deterministic PDE for each input spectral mode [19, 20], as depicted schematically in Figure 2. The robustness and scalability issues in the SSP method arise from the application of sampling around the deterministic PDE solvers.

Recently, another UQ approach that applies sampling around deterministic residuals, Jacobians, initial conditions instead of the entire PDE solution module, has been developed by the authors [50, 51] in the context of FEM for flexible multibody dynamics, and by Chatzimanolakis *et al.* [52] in the context of finite volume methods for Navier–Stokes equations. The method is illustrated schematically in Figure 2. In our method, the discretized SPDE equations are assembled by sampling the discretized deterministic PDE at a set of nodes from the probabilistic domain. The advantages of this approach over the other UQ methods are enumerated below:

1) It enables the reuse of discretization methods implemented for the deterministic PDE and alleviates the issue of intrusiveness with the classical SGM implementations.
2) The method does not inherit the solver robustness issues like the SSM or SSP, as it does not rely on deterministic solutions of the PDE.

Regarding the applicability of our concept, it can be used for the implementation of the adjoint sensitivity analysis for OUU applications, or to extract the block-sparse matrices and vectors from deterministic PDE frameworks to cater studies focusing on the scalability of solving SPDE linear systems [44–49] on a broader class of SPDE models.

The novelties and contributions of this work are: (1) the placement of sampling to surround deterministic space-time discretizations for simplifying the stochastic PDE and adjoint implementation, (2) software architectures describing the implementation of stochastic FEM as an extension of deterministic FEM, and (3) OUU demonstrations with SGM adjoint derivatives of the statistics.

In the remainder of this article, we focus on the formulation, implementation, verification, and OUU applications of our semi-intrusive SGM in the context of FEM, flexible multibody dynamics, and adjoint sensitivity analysis. In Section II we review the solution of OUU problems using SSM. In Section III, we describe the mathematical formulation of our semi-intrusive SGM for time-dependent physics and adjoint sensitivity analysis. In Section IV, we present software architectures to implement SGM. In Section V, we present verification studies and OUU applications using the stochastic framework. Section VI concludes the article.

II. Optimization Under Uncertainty Using Stochastic Sampling Methods

The deterministic optimization procedure involves a *forward-mode* analysis of physics and a *reverse-mode* sensitivity analysis implementation such as the adjoint method as depicted in Figure 1, whereas in the presence of uncertainty analysis, the problem statement evolves into an expanded context as optimization under uncertainty.

A. Deterministic PDE and Optimization

In the context of flexible multibody dynamics, we consider the solution of the Euler–Lagrange equations of motion [53]:

$$\boldsymbol{R}(\boldsymbol{x}, t; \boldsymbol{u}(\boldsymbol{x}, t)) = \boldsymbol{0}, \tag{1}$$

where $\boldsymbol{u}(\boldsymbol{x}, t)$ are the state variables that depend on time $t \in \mathcal{T}$ and the design variables $\boldsymbol{x} \in \mathcal{D}$. Here, the time derivatives $\dot{\boldsymbol{u}}(\boldsymbol{x}, t)$ and $\ddot{\boldsymbol{u}}(\boldsymbol{x}, t)$, as well as the dependence of $\boldsymbol{u}$ on the spatial domain are suppressed for simplicity of notation. In this work, we use the overloaded notation $\boldsymbol{R}$ to also refer to the residuals of the system of equations in the context of Newton–Raphson method.

We consider output functions of the form $F(\boldsymbol{x}, t; \boldsymbol{u}(\boldsymbol{x}, t))$ that denote time-dependent fields such as displacement, stress, and strain. These output fields may be averaged over an interval of time as

$$\bar{F}(\boldsymbol{x}) = \frac{1}{t_f - t_0} \int_{t_0}^{t_f} F(\boldsymbol{x}, t; \boldsymbol{u}(\boldsymbol{x}, t))\, dt, \tag{2}$$

or, their maximum over a time interval may be estimated using the Kreisselmeier–Steinhauser (KS) aggregation method [54, 55] as

$$\bar{F}(\boldsymbol{x}) = c_{ks} + \frac{1}{\rho_{ks}} \ln \int_{t_0}^{t_f} \exp\left[\rho_{ks}\left(F(\boldsymbol{x}, t; \boldsymbol{u}(\boldsymbol{x}, t)) - c_{ks}\right)\right]\, dt. \tag{3}$$

The parameters ρ_{ks} and c_{ks} in Eq. (3) are used to control the accuracy of the estimates. The functions (2) or (3) or other functions of F are used to formulate the objective $f(\boldsymbol{x})$ and constraints functions $\boldsymbol{c}(\boldsymbol{x})$ of deterministic optimization problems based on the design context. For example, a single objective deterministic optimization can be formulated as

$$\begin{aligned} \underset{\boldsymbol{x} \in \mathcal{D}}{\text{minimize}} \quad & f(\boldsymbol{x}) \triangleq \bar{F}(\boldsymbol{x}) \\ \text{subject to} \quad & \boldsymbol{c}(\boldsymbol{x}) \triangleq \bar{C}(\boldsymbol{x}) \leq 0. \end{aligned} \tag{4}$$

The derivatives $df(\boldsymbol{x})/d\boldsymbol{x}$ and $d\boldsymbol{c}(\boldsymbol{x})/d\boldsymbol{x}$ are evaluated by applying the adjoint method [56, 57] for scalability in terms of the number of design variables.

B. Stochastic PDE and Optimization Under Uncertainty

In the presence probabilistically modeled random variable inputs $\boldsymbol{y}$, we consider the solution of the stochastic PDEs as solving the following system of nonlinear equations

$$\mathbf{R}(\boldsymbol{x}, t, \boldsymbol{y}; \mathbf{u}(\boldsymbol{x}, t, \boldsymbol{y})) = \mathbf{0}, \tag{5}$$

where $\mathbf{u}(\boldsymbol{x}, t, \boldsymbol{y})$ are the stochastic state variables. Throughout this work, we use the terms *stochastic*, *random* and *probabilistic* to refer to the dependence of functions on the probabilistic random coordinate $\boldsymbol{y}$ (in a sense similar to the temporal coordinate $t \in \mathcal{T}$), and *deterministic* to refer to functions that lack this dependence.

Similar to the deterministic output (2), the time-averaged probabilistic output fields are

$$\bar{\mathsf{F}}(\boldsymbol{x},\boldsymbol{y}) = \frac{1}{t_f - t_0}\int_{t_0}^{t_f} \mathsf{F}(\boldsymbol{x},t,\boldsymbol{y};\mathbf{u}(\boldsymbol{x},t,\boldsymbol{y}))\,dt, \tag{6}$$

or, their temporal maximum are

$$\bar{\mathsf{F}}(\boldsymbol{x},\boldsymbol{y}) = c_{ks} + \frac{1}{\rho_{ks}}\ln\int_{t_0}^{t_f} \exp\left[\rho_{ks}\left(\mathsf{F}(\boldsymbol{x},t,\boldsymbol{y};\mathbf{u}(\boldsymbol{x},t,\boldsymbol{y})) - c_{ks}\right)\right]\,dt. \tag{7}$$

The statistical measures such as the expectation $\mathbb{E}[\bar{\mathsf{F}}(\boldsymbol{x},\boldsymbol{y})]$, variance $\mathbb{V}[\bar{\mathsf{F}}(\boldsymbol{x},\boldsymbol{y})]$, and standard deviation $\mathbb{S}[\bar{\mathsf{F}}(\boldsymbol{x},\boldsymbol{y})]$, are utilized in OUU problem formulations. In this investigation, we consider the robust optimization problem formulation among other variants [1, 8, 39]

$$\begin{aligned} \underset{\boldsymbol{x}\in\mathcal{D}}{\text{minimize}} \quad & f(\boldsymbol{x}) \triangleq \mathbb{E}[\bar{\mathsf{F}}(\boldsymbol{x},\boldsymbol{y})] + \mathbb{S}[\bar{\mathsf{F}}(\boldsymbol{x},\boldsymbol{y})] \\ \text{subject to} \quad & \boldsymbol{c}(\boldsymbol{x}) \triangleq \mathbb{E}[\bar{\mathbf{C}}(\boldsymbol{x},\boldsymbol{y})] + K\cdot\mathbb{S}[\bar{\mathbf{C}}(\boldsymbol{x},\boldsymbol{y})] \leq 0. \end{aligned} \tag{8}$$

In contrast to the deterministic optimization (4), the OUU objective function $f(\boldsymbol{x})$ includes the expectation and a measure of its variability. The constraint $\boldsymbol{c}(\boldsymbol{x})$ demands that the design output $\boldsymbol{x}$ observes a separation of K standard deviations from the expected constraint manifold. To utilize gradient-based algorithms for optimization, we consider the evaluation of the adjoint derivatives of statistical measures:

$$\frac{d\mathbb{E}[\bar{\mathsf{F}}(\boldsymbol{x},\boldsymbol{y})]}{d\boldsymbol{x}}, \frac{d\mathbb{V}[\bar{\mathsf{F}}(\boldsymbol{x},\boldsymbol{y})]}{d\boldsymbol{x}} \text{ and } \frac{d\mathbb{S}[\bar{\mathsf{F}}(\boldsymbol{x},\boldsymbol{y})]}{d\boldsymbol{x}}. \tag{9}$$

C. Stochastic Sampling Method and Adjoint Derivatives

The stochastic sampling method requires the solution of deterministic PDEs for all the probabilistic nodes $\boldsymbol{y}_q$ provided by the sampling scheme resulting in the solution of the nonlinear system as follows

$$\boldsymbol{R}(\boldsymbol{x},t,\boldsymbol{y}_q;\boldsymbol{u}(\boldsymbol{x},t,\boldsymbol{y}_q)) = \mathbf{0}. \tag{10}$$

Throughout this work, we utilize the tensor-product quadrature nodes and weights $\{\boldsymbol{y}_q,\alpha_q\}_{q=1}^{Q}$ normalized such that $\sum_{q=1}^{Q}\alpha_q = 1$. These nodes are the roots of the polynomials associated with the input probability distributions listed in Table 1 for better rates of convergence. The output functions (6) and (7) are evaluated at these quadrature nodes to evaluate their expectation as

$$\mathbb{E}[\bar{\mathsf{F}}(\boldsymbol{x},\boldsymbol{y})] \triangleq \int_{\mathcal{Y}} \rho(\boldsymbol{y})\bar{\mathsf{F}}(\boldsymbol{x},\boldsymbol{y})\,\mathrm{d}\boldsymbol{y} = \sum_{q=1}^{Q}\alpha_q\bar{F}(\boldsymbol{x},\boldsymbol{y}_q), \tag{11}$$

and the variance as

$$\mathbb{V}[\bar{\mathsf{F}}(\boldsymbol{x},\boldsymbol{y})] \triangleq \mathbb{E}[\bar{\mathsf{F}}(\boldsymbol{x},\boldsymbol{y})^2] - \mathbb{E}[\bar{\mathsf{F}}(\boldsymbol{x},\boldsymbol{y})]^2 = \sum_{q=1}^{Q} \alpha_q \bar{F}(\boldsymbol{x},\boldsymbol{y}_q)^2 - \mathbb{E}[\bar{\mathsf{F}}(\boldsymbol{x},\boldsymbol{y})]^2. \tag{12}$$

Similar to the statistics, the derivatives of the expectation are formed through quadrature sampling as

$$\frac{d\mathbb{E}[\bar{\mathsf{F}}(\boldsymbol{x},\boldsymbol{y})]}{d\boldsymbol{x}} = \mathbb{E}\left[\frac{d\bar{\mathsf{F}}(\boldsymbol{x},\boldsymbol{y})}{d\boldsymbol{x}}\right] = \int_{\mathcal{Y}} \rho(\boldsymbol{y}) \frac{d\bar{\mathsf{F}}(\boldsymbol{x},\boldsymbol{y})}{d\boldsymbol{x}}\, \mathrm{d}\boldsymbol{y} = \sum_{q=1}^{Q} \alpha_q \frac{d\bar{F}(\boldsymbol{x},\boldsymbol{y}_q)}{d\boldsymbol{x}}, \tag{13}$$

and the derivatives of the variance as

$$\frac{d\mathbb{V}[\bar{\mathsf{F}}(\boldsymbol{x},\boldsymbol{y})]}{d\boldsymbol{x}} = 2\sum_{q=1}^{Q} \alpha_q \bar{F}(\boldsymbol{x},\boldsymbol{y}_q) \frac{d\bar{F}(\boldsymbol{x},\boldsymbol{y}_q)}{d\boldsymbol{x}} - 2\,\mathbb{E}[\bar{\mathsf{F}}(\boldsymbol{x},\boldsymbol{y})] \frac{d\mathbb{E}[\bar{\mathsf{F}}(\boldsymbol{x},\boldsymbol{y})]}{d\boldsymbol{x}}. \tag{14}$$

The standard deviation and its derivatives are obtained using the relation $\mathbb{S}[\bar{\mathsf{F}}] = \sqrt{\mathbb{V}[\bar{\mathsf{F}}]}$. Note that in Eqs. (13) and (14) the derivative operator is moved inside the integral making use of our assumption that the probabilistic variables $\boldsymbol{y}$ and the integration limits are independent of the design variables $\boldsymbol{x}$. We implement probabilistic sampling around deterministic physics and adjoint frameworks for non-intrusive formation of (11)–(14) as a benchmark to verify the same quantities evaluated by implementing the semi-intrusive SGM.

Table 1 The probability density functions, basis polynomials and quadrature rules for distribution types.

Distribution	Density function $\rho(y)$	Univariate orthonormal polynomials $\psi_k(\mathrm{y})$	Quadrature rule
Gaussian $\mathcal{N}$	$\frac{1}{\sigma\sqrt{2\pi}} \exp[-\frac{1}{2}(\frac{y-\mu}{\sigma})^2]$	$1, \left(\frac{y-\mu}{\sigma}\right), \left((\frac{y-\mu}{\sigma})^2 - 1\right)/2!, \ldots$	Gauss–Hermite
Uniform $\mathcal{U}$	$\frac{1}{b-a}$	$1, \left(2(\frac{y-a}{b-a}) - 1\right)\sqrt{3}, \left(6(\frac{y-a}{b-a})^2 - 6(\frac{y-a}{b-a}) + 1\right)\sqrt{5}, \ldots$	Gauss–Legendre
Exponential $\mathcal{E}$	$\frac{1}{\beta} \exp[-(\frac{y-\mu}{\beta})]$	$1, 1 - (\frac{y-\mu}{\beta}), \left(2 - 4(\frac{y-\mu}{\beta}) + (\frac{y-\mu}{\beta})^2\right)/2!, \ldots$	Gauss–Laguerre

III. Semi-Intrusive Stochastic Galerkin Method

Consider a set of basis functions $\boldsymbol{\psi}(\boldsymbol{y}) = \{\psi_1(\boldsymbol{y}), \psi_2(\boldsymbol{y}), \ldots, \psi_N(\boldsymbol{y})\}$ for M-dimensional random variable $\boldsymbol{y} = [y_1, y_2, \ldots, y_M]$. The basis functions are constructed orthonormal to each other with respect to the probability density function for simpler recovery of decomposition coefficients as

$$\left\langle \psi_i(\boldsymbol{y}) \,\middle|\, \psi_j(\boldsymbol{y}) \right\rangle_{\rho(\boldsymbol{y})}^{\mathcal{Y}} = \int_{\mathcal{Y}} \rho(\boldsymbol{y}) \psi_i(\boldsymbol{y}) \psi_j(\boldsymbol{y})\, d\boldsymbol{y} = \delta_{ij}, \tag{15}$$

where δ_{ij} is the Kronecker delta function. The multivariate basis entries of the set $\boldsymbol{\psi}(\boldsymbol{y})$ are constructed from the univariate polynomials listed in Table 1. Each of the P deterministic degrees of freedom in the deterministic finite

element model and the corresponding governing kinematic, dynamic, constraint laws in the flexible multibody system are associated with N probabilistic spectral degrees of freedom and forms the stochastic Galerkin finite element model (see Figure 3). For efficient basis selection, it may be necessary to consider generalization schemes other than tensor products, similar in principle to adaptive sampling methods [35].

	ψ_1	ψ_2	$\dots$	ψ_N
R_1	$R_1 \times \psi_1$	$R_1 \times \psi_2$	$\dots$	$R_1 \times \psi_N$
R_2	$R_2 \times \psi_1$	$R_2 \times \psi_2$	$\dots$	$R_2 \times \psi_N$
$\vdots$	$\vdots$	$\vdots$	$\ddots$	$\vdots$
R_P	$R_P \times \psi_1$	$R_P \times \psi_2$	$\dots$	$R_P \times \psi_N$
$\boldsymbol{R}$	$\boldsymbol{R} \times \psi_1$	$\boldsymbol{R} \times \psi_2$	$\dots$	$\boldsymbol{R} \times \psi_N$
	$\mathbf{R} \triangleq \boldsymbol{R} \otimes \boldsymbol{\psi}$			

	ψ_1	ψ_2	$\dots$	ψ_N
u_1	$u_1 \times \psi_1$	$u_1 \times \psi_2$	$\dots$	$u_1 \times \psi_N$
u_2	$u_2 \times \psi_1$	$u_2 \times \psi_2$	$\dots$	$u_2 \times \psi_N$
$\vdots$	$\vdots$	$\vdots$	$\ddots$	$\vdots$
u_P	$u_P \times \psi_1$	$u_P \times \psi_2$	$\dots$	$u_P \times \psi_N$
$\boldsymbol{u}$	$\boldsymbol{u} \times \psi_1$	$\boldsymbol{u} \times \psi_2$	$\dots$	$\boldsymbol{u} \times \psi_N$
	$\mathbf{u} \triangleq \boldsymbol{u} \otimes \boldsymbol{\psi}$			

Fig. 3 The tensor product of deterministic residuals and state variables with the probabilistic basis set forms the stochastic residuals and states in the forward-problem. This generalization scheme is applicable to the adjoint reverse-problem as well as other functions of the random variable.

A. Solution of Stochastic Governing Equations

Consider the decomposition of a function $a(\boldsymbol{y})$ in terms of another function $b(\boldsymbol{y})$ in the probabilistic domain $\mathcal{Y}$ defined as weighted inner product

$$\Big\langle a(\boldsymbol{y}) \,\Big|\, b(\boldsymbol{y}) \Big\rangle_{\rho(\boldsymbol{y})}^{\mathcal{Y}} \triangleq \int_{\mathcal{Y}} a(\boldsymbol{y})\, \rho(\boldsymbol{y})\, b(\boldsymbol{y})\, d\boldsymbol{y} = \sum_{q=1}^{Q} a(\boldsymbol{y}_q)\, \alpha_q\, b(\boldsymbol{y}_q). \tag{16}$$

By applying this decomposition operator to the stochastic functions of $\boldsymbol{y}$ listed in Table 2, all the terms needed for the implementation of SGM can be obtained *numerically* through the sampling of the underlying deterministic residual, Jacobian, initial conditions, and adjoint implementations. We formulate the Newton–Raphson iterative procedure for the solution of nonlinear system (5) applying linearization in terms of the unknown state variables $\mathbf{u}$ resulting in linear system of the form:

$$\begin{bmatrix} \mathbf{J}_{11} & \mathbf{J}_{12} & \dots & \mathbf{J}_{1N} \\ \mathbf{J}_{21} & \mathbf{J}_{22} & \dots & \mathbf{J}_{2N} \\ \vdots & \vdots & \ddots & \vdots \\ \mathbf{J}_{N1} & \mathbf{J}_{N2} & \dots & \mathbf{J}_{NN} \end{bmatrix} \begin{Bmatrix} \Delta\mathbf{u}_1 \\ \Delta\mathbf{u}_2 \\ \vdots \\ \Delta\mathbf{u}_N \end{Bmatrix} = - \begin{Bmatrix} \mathbf{R}_1 \\ \mathbf{R}_2 \\ \vdots \\ \mathbf{R}_N \end{Bmatrix}. \tag{17}$$

The linearized SPDE system of coefficients (17) is solved to obtain stochastic state updates

$$\mathbf{u}^{n+1} = \mathbf{u}^n + \Delta\mathbf{u}^n. \tag{18}$$

The Newton–Raphson iterations are repeated until the norm of residuals are under a certain tolerance. The residual vector and Jacobian matrix of the linear system (17) is assembled through the sampling of deterministic residuals

$$\mathbf{R}_j \triangleq \left\langle \psi_j(\boldsymbol{y}) \,\middle|\, \mathbf{R}(\boldsymbol{x}, t, \boldsymbol{y}; \mathbf{u}(\boldsymbol{x}, t, \boldsymbol{y})) \right\rangle_{\rho(\boldsymbol{y})}^{\mathcal{Y}} = \sum_{q=1}^{Q} \alpha_q \, \psi_j(\boldsymbol{y}_q) \boldsymbol{R}(\boldsymbol{x}, t, \boldsymbol{y}_q; \boldsymbol{u}(\boldsymbol{x}, t, \boldsymbol{y}_q)). \tag{19}$$

Similarly, the Jacobian terms in the linear system (17) are obtained by sampling the deterministic Jacobian

$$\mathbf{J}_{jk} \triangleq \left\langle \psi_j(\boldsymbol{y}) \,\middle|\, \frac{\partial \mathbf{R}}{\partial \mathbf{u}} (\boldsymbol{x}, t, \boldsymbol{y}; \mathbf{u}(\boldsymbol{x}, t, \boldsymbol{y})) \,\middle|\, \psi_k(\boldsymbol{y}) \right\rangle_{\rho(\boldsymbol{y})}^{\mathcal{Y}} = \sum_{q=1}^{Q} \alpha_q \, \psi_j(\boldsymbol{y}_q) \frac{\partial \boldsymbol{R}}{\partial \boldsymbol{u}} \left(\boldsymbol{x}, t, \boldsymbol{y}_q; \boldsymbol{u}(\boldsymbol{x}, t, \boldsymbol{y}_q)\right) \psi_k(\boldsymbol{y}_q). \tag{20}$$

The stochastic state vector of size $N \times P$ available as the Newton–Raphson iterate (18) is linearly-combined with N stochastic basis functions evaluated at the quadrature nodes to form the deterministic state vector of size P as

$$\boldsymbol{u}(\boldsymbol{x}, t, \boldsymbol{y}_q) = \sum_{i=1}^{N} \mathbf{u}_i(\boldsymbol{x}, t) \, \psi_i(\boldsymbol{y}_q). \tag{21}$$

This deterministic state vector is needed as input to the deterministic framework for the evaluation of the deterministic residual and Jacobians at each quadrature point $\boldsymbol{y}_q$ in Eqs. (19) and (20) This principle is applied to form the time derivatives of the deterministic states $\dot{\boldsymbol{u}}$ and $\ddot{\boldsymbol{u}}$, as well the adjoint state variables $\boldsymbol{v}$ and $\boldsymbol{w}$ for the sensitivity analysis. For time-dependent simulations, the stochastic initial conditions vector is formed in a manner similar to the stochastic residuals through the probabilistic sampling of deterministic initial condition implementations at $t = t_0$ as

$$\mathbf{u}_j(\boldsymbol{x}, t_0) \triangleq \left\langle \psi_j(\boldsymbol{y}) \,\middle|\, \mathbf{u}(\boldsymbol{x}, t_0, \boldsymbol{y}) \right\rangle = \sum_{q=1}^{Q} \alpha_q \, \psi_j(\boldsymbol{y}_q) \boldsymbol{u}(\boldsymbol{x}, t_0, \boldsymbol{y}_q). \tag{22}$$

The indices j, k in Eqs (19), (20), (22) run from 1 to N through the set of stochastic basis functions. The stochastic states, residuals, and Jacobian are N times larger than their deterministic counterparts, due to the association of N spectral modes to each deterministic degree of freedom as shown in Figure 3. Note that the finite element connectivities and spatial and temporal discretization nodes remain the same in the stochastic finite element problem. As an illustrative example, Figure 4 depicts the stochastic Jacobian sparsity patterns of a simple one degree of freedom ($P = 1$) spring model after stochastic decomposition using Eq. 20 with $N = 343$ basis functions. This method can be applied to extract more complicated sparsity patterns associated with flexible multibody systems or other physics.

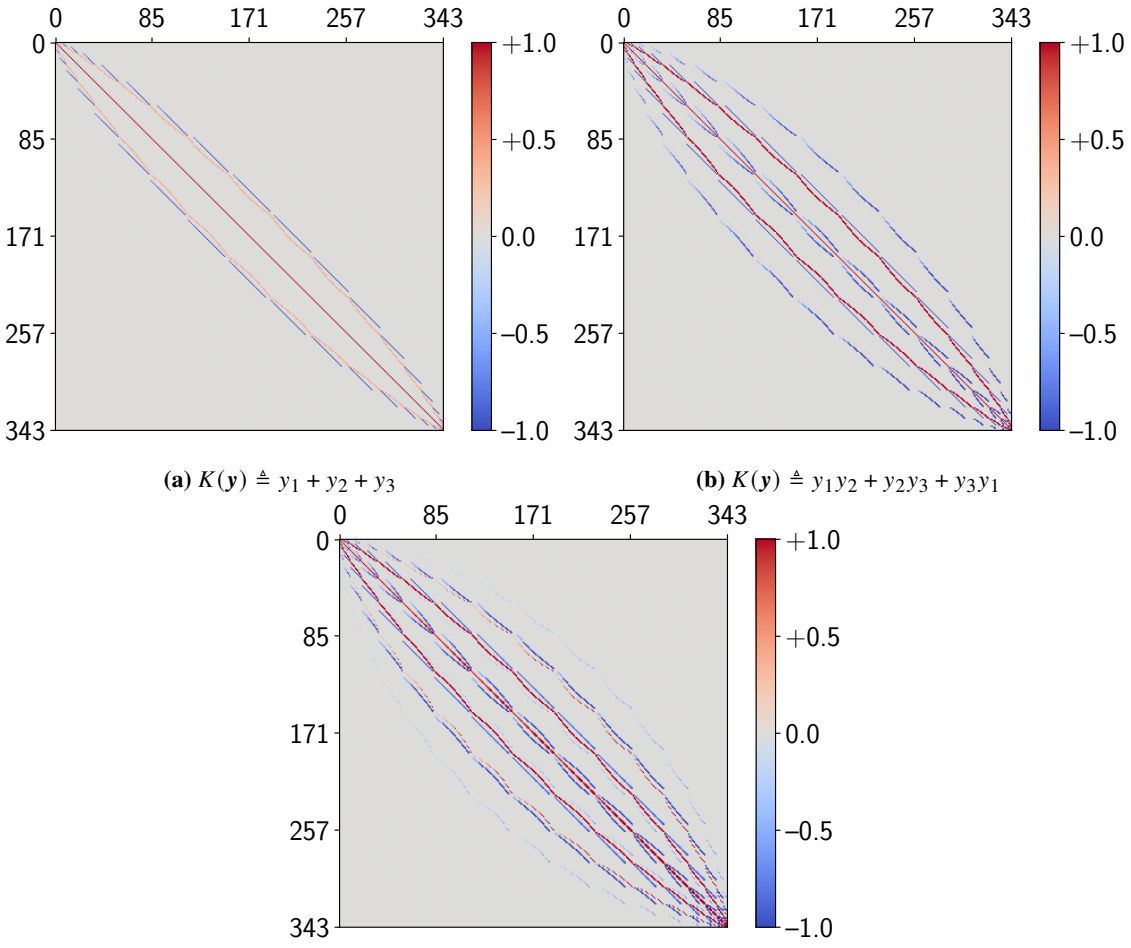

(a) $K(\boldsymbol{y}) \triangleq y_1 + y_2 + y_3$

(b) $K(\boldsymbol{y}) \triangleq y_1y_2 + y_2y_3 + y_3y_1$

(c) $K(\boldsymbol{y}) \triangleq y_1y_2y_3$

Fig. 4 Nonzero patterns of the stochastic stiffness matrix for a spring with stiffness $\mathsf{K}(y_1, y_2, y_3)$ where $y_1 \sim \mathcal{E}(\mu = \pi/2, \beta = \pi/4)$, $y_2 \sim \mathcal{N}(\mu = \pi/2, \sigma = \pi/20)$, and $y_3 \sim \mathcal{U}(a = \pi/4, b = 3\pi/4)$. The spectral basis set is formed through the tensor-product of the first seven Laguerre, Hermite, and Legendre polynomials.

B. Statistical Measures

The stochastic functions $\bar{\mathsf{F}}(\boldsymbol{x}, \boldsymbol{y})$ are decomposed into the bases and coefficients through the sampling of deterministic function implementation as

$$\bar{\mathsf{F}}_j(\boldsymbol{x}) \triangleq \left\langle \psi_j(\boldsymbol{y}) \,\middle|\, \bar{\mathsf{F}}(\boldsymbol{x}, \boldsymbol{y}) \right\rangle_{\rho(\boldsymbol{y})}^{\boldsymbol{y}} = \sum_{q=1}^{Q} \alpha_q \psi_j(\boldsymbol{y}_q) \bar{F}(\boldsymbol{x}, \boldsymbol{y}_q). \tag{23}$$

The expectation and variance are obtained directly from the decomposition coefficients $\bar{\mathsf{F}}_j$, where the expectation is

$$\mathbb{E}[\bar{\mathsf{F}}(\boldsymbol{x}, \boldsymbol{y})] = \bar{\mathsf{F}}_1(\boldsymbol{x}), \tag{24}$$

and the variance is

$$\mathbb{V}[\bar{\mathsf{F}}(\boldsymbol{x},\boldsymbol{y})] = \mathbb{E}[\bar{\mathsf{F}}(\boldsymbol{x},\boldsymbol{y})^2] - \mathbb{E}[\bar{\mathsf{F}}(\boldsymbol{x},\boldsymbol{y})]^2 = \sum_{j=2}^{N} \bar{\mathsf{F}}_j^2(\boldsymbol{x}). \tag{25}$$

The SGM statistics (24) and (25) can be evaluated through the sampling of deterministic function outputs as outlined in Eq. (23).

C. Stochastic Galerkin Adjoint Derivatives

Next, we present the stochastic Galerkin adjoint formulation to evaluate the design variable derivatives of the expectation (24) and variance (25) based on the sampling of deterministic adjoint implementation [56]. The derivative of the expectation is obtained as

$$\frac{d\mathbb{E}[\bar{\mathsf{F}}(\boldsymbol{x},\boldsymbol{y})]}{d\boldsymbol{x}} = \left\langle \psi_1(\boldsymbol{y}) \,\middle|\, \frac{d\bar{\mathsf{F}}(\boldsymbol{x},\boldsymbol{y})}{d\boldsymbol{x}} \right\rangle_{\rho(\boldsymbol{y})}^{\mathcal{Y}} = \sum_{q=1}^{Q} \alpha_q \psi_1(\boldsymbol{y}_q) \frac{d\bar{F}(\boldsymbol{x},\boldsymbol{y}_q)}{d\boldsymbol{x}}. \tag{26}$$

Eq. (26) employs the sampling of the assembled deterministic derivative $d\bar{F}(\boldsymbol{x},\boldsymbol{y}_q)/d\boldsymbol{x}$. The total derivative implemented within the deterministic framework takes the form

$$\frac{d\bar{F}(\boldsymbol{x},\boldsymbol{y}_q)}{d\boldsymbol{x}} = \frac{\partial \bar{F}(\boldsymbol{x},\boldsymbol{y}_q)}{\partial \boldsymbol{x}} + \boldsymbol{v}^T(\boldsymbol{y}_q) \frac{\partial \boldsymbol{R}(\boldsymbol{x},\boldsymbol{y}_q;\boldsymbol{u}(\boldsymbol{x},\boldsymbol{y}_q))}{\partial \boldsymbol{x}}, \tag{27}$$

due to the adjoint decomposition [56]. Note that the deterministic adjoint variables $\boldsymbol{v}$ at $\boldsymbol{y}_q$ are needed for Eq. (27) as input to the deterministic framework along with the state inputs $\boldsymbol{u}$ at $\boldsymbol{y}_q$ to obtain the assembled derivative. We form the deterministic adjoint variables $\boldsymbol{v}$ from the stochastic adjoint variables $\mathbf{v}$ in a manner similar to the forward physics as outlined in Eq. (21). The stochastic adjoint states $\mathbf{v}$ are found by solving the linear system

$$\begin{bmatrix} \mathbf{J}_{11}^{\mathrm{T}} & \dots & \mathbf{J}_{1N}^{\mathrm{T}} \\ \vdots & \vdots & \vdots \\ \mathbf{J}_{N1}^{\mathrm{T}} & \dots & \mathbf{J}_{NN}^{\mathrm{T}} \end{bmatrix} \begin{Bmatrix} \mathbf{v}_1 \\ \vdots \\ \mathbf{v}_N \end{Bmatrix} = - \begin{Bmatrix} \sum_{q=1}^{Q} \alpha_q \psi_1(\boldsymbol{y}_q) \dfrac{\partial \bar{F}(\boldsymbol{x},\boldsymbol{y}_q)}{\partial \boldsymbol{u}} \\ \vdots \\ \sum_{q=1}^{Q} \alpha_q \psi_N(\boldsymbol{y}_q) \dfrac{\partial \bar{F}(\boldsymbol{x},\boldsymbol{y}_q)}{\partial \boldsymbol{u}} \end{Bmatrix}. \tag{28}$$

To assemble the linear adjoint system (28), we use Eq. (20) for the formation of the Jacobian. The right hand side is formed through the sampling of the deterministic implementation as follows

$$\left\langle \psi_k(\boldsymbol{y}) \,\middle|\, \frac{\partial \bar{\mathsf{F}}(\boldsymbol{x},\boldsymbol{y}_q)}{\partial \mathbf{u}} \right\rangle = \sum_{q=1}^{Q} \alpha_q \psi_k(\boldsymbol{y}_q) \frac{\partial \bar{F}(\boldsymbol{x},\boldsymbol{y}_q)}{\partial \boldsymbol{u}}. \tag{29}$$

Next, the total derivative of the variance is decomposed into two components based on the identity (12) as

$$\begin{aligned}\frac{d\mathbb{V}[\bar{\mathsf{F}}(\boldsymbol{x},\boldsymbol{y})]}{d\boldsymbol{x}} &= \frac{d\mathbb{E}[\bar{\mathsf{F}}^2(\boldsymbol{x},\boldsymbol{y})]}{d\boldsymbol{x}} - 2\mathbb{E}[\bar{\mathsf{F}}(\boldsymbol{x},\boldsymbol{y})]\frac{d\mathbb{E}[\bar{\mathsf{F}}(\boldsymbol{x},\boldsymbol{y})]}{d\boldsymbol{x}} \\ &= \left\langle \psi_1(\boldsymbol{y}) \,\middle|\, \frac{d\bar{\mathsf{F}}^2(\boldsymbol{x},\boldsymbol{y})}{d\boldsymbol{x}} \right\rangle_{\rho(y)}^{\mathcal{Y}} - 2\left\langle \psi_1(\boldsymbol{y}) \,\middle|\, \bar{\mathsf{F}}(\boldsymbol{x},\boldsymbol{y}) \right\rangle_{\rho(y)}^{\mathcal{Y}} \left\langle \psi_1(\boldsymbol{y}) \,\middle|\, \frac{d\bar{\mathsf{F}}(\boldsymbol{x},\boldsymbol{y})}{d\boldsymbol{x}} \right\rangle_{\rho(y)}^{\mathcal{Y}}.\end{aligned} \tag{30}$$

The second component is available at this stage and therefore we apply the adjoint decomposition method for the *squared output function* $\bar{\mathsf{F}}^2$, and follow the same approach outlined for the expectation of $\bar{\mathsf{F}}$. The total derivative of the squared output is formed by sampling the deterministic implementation as

$$\frac{d\bar{F}^2(\boldsymbol{x},\boldsymbol{y}_q)}{d\boldsymbol{x}} = \frac{\partial\bar{F}^2(\boldsymbol{x},\boldsymbol{y}_q)}{\partial\boldsymbol{x}} + \boldsymbol{w}^T(\boldsymbol{y}_q)\frac{\partial\boldsymbol{R}(\boldsymbol{x},\boldsymbol{y}_q;\boldsymbol{u}(\boldsymbol{x},\boldsymbol{y}_q))}{\partial\boldsymbol{x}}. \tag{31}$$

We use the chain-rule $\partial\bar{F}^2(\boldsymbol{x},\boldsymbol{y}_q)/\partial\boldsymbol{x} = 2\,\bar{F}(\boldsymbol{x},\boldsymbol{y}_q)\,\partial\bar{F}(\boldsymbol{x},\boldsymbol{y}_q)/\partial\boldsymbol{x}$ for reusing the available deterministic implementation for the function and its partial derivatives. The adjoint linear system of equations for the adjoint variables $\mathbf{w}$ is

$$\begin{bmatrix} \mathbf{J}_{11}^{\mathrm{T}} & \dots & \mathbf{J}_{1N}^{\mathrm{T}} \\ \vdots & \vdots & \vdots \\ \mathbf{J}_{N1}^{\mathrm{T}} & \dots & \mathbf{J}_{NN}^{\mathrm{T}} \end{bmatrix} \begin{Bmatrix} \mathbf{w}_1 \\ \vdots \\ \mathbf{w}_N \end{Bmatrix} = -\begin{Bmatrix} \sum_{q=1}^{Q}\alpha_q\psi_1(\boldsymbol{y}_q)\dfrac{\partial\bar{F}^2(\boldsymbol{x},\boldsymbol{y}_q)}{\partial\boldsymbol{u}} \\ \vdots \\ \sum_{q=1}^{Q}\alpha_q\psi_N(\boldsymbol{y}_q)\dfrac{\partial\bar{F}^2(\boldsymbol{x},\boldsymbol{y}_q)}{\partial\boldsymbol{u}} \end{Bmatrix}. \tag{32}$$

The right-hand-side (32) may apply the chain-rule: $\partial\bar{F}^2(\boldsymbol{x},\boldsymbol{y}_q)/\partial\boldsymbol{u} = 2\,\bar{F}(\boldsymbol{x},\boldsymbol{y}_q)\,\partial\bar{F}(\boldsymbol{x},\boldsymbol{y}_q)/\partial\boldsymbol{u}$ for reusing the available deterministic implementation.

The above formulation is presented from the perspective of a static finite-element adjoint method. The adjoint for time-dependent systems can be obtained by sampling the time-dependent deterministic adjoint implementation. The linear systems and the formation of total derivatives then involve the derivatives of the integrand and the appropriate temporal scaling factor [56].

As a method of verification of the stochastic Galerkin implementation, note that if $N = 1$ the deterministic finite element vectors, matrices, and derivatives must be recovered. This property can be used as one of the verification steps after the stochastic finite element and adjoint implementation. In addition, one can verify the consistency of stochastic residuals with the stochastic Jacobians using the complex-step perturbations of the stochastic state variables.

IV. Software Architecture for Stochastic Galerkin Method

A key advantage of the proposed semi-intrusive SGM technique is that it can be implemented using straightforward software architectures that leverage existing deterministic finite element frameworks. In this section, we describe the software architecture related details of our stochastic finite element implementation that extends the TACS [56, 58]

Table 2 The terms required for the implementation of a stochastic finite element framework from deterministic finite element implementations, along with adjoint sensitivity analysis for expectation, variance, and standard deviation operators.

	Operators	State Variable Sensitivities	Design Variable Sensitivities
Stochastic	R	$\partial\mathsf{R}/\partial\mathsf{u}$	$\partial\mathsf{R}/\partial\boldsymbol{x}$
Deterministic	$\boldsymbol{R}$	$\partial\boldsymbol{R}/\partial\boldsymbol{u}$	$\partial\boldsymbol{R}/\partial\boldsymbol{x}$
Stochastic	F	$\partial\mathsf{F}/\partial\mathsf{u}$	$\partial\mathsf{F}/\partial\boldsymbol{x}$
Deterministic	F	$\partial F/\partial\boldsymbol{u}$	$\partial F/\partial\boldsymbol{x}$
Stochastic	F^2	$\partial\mathsf{F}^2/\partial\mathsf{u}$	$\partial\mathsf{F}^2/\partial\boldsymbol{x}$
Deterministic	F^2	$\partial F^2/\partial\boldsymbol{u}$	$\partial F^2/\partial\boldsymbol{x}$

deterministic finite element framework. The description is centered around abstract mathematical operators and derivatives listed in Table 2 that are PDE framework and physics agnostic.

A. Deterministic Finite Element Framework for Physics and Adjoint Sensitivity Analysis

Consider the deterministic finite element framework to consist of the following components:

1) An `Element` interface to organize element-level block computations based on abstract form $\boldsymbol{R}_e(\boldsymbol{x}_e, t; \boldsymbol{u}_e(\boldsymbol{x}_e, t))$ and its state and design derivatives listed in Table 2. The classes implementing this `Element` interface apply the spatial discretization methods for beams, shells, solids, rigid bodies, and kinematic constraints, and their derivatives.

   A `Function` interface organizes the evaluation of output quantities of interest and their derivatives based on abstract form $F_e(\boldsymbol{x}_e, t; \boldsymbol{u}_e(\boldsymbol{x}_e, t))$. The classes implementing this `Function` interface evaluate the element-level stresses, deformations, compliance, structural mass, and other physical quantities, and their derivatives.

2) An `Assembler` class collects the blocks of element residual arrays $\boldsymbol{R}_e$, Jacobian matrices $\partial\boldsymbol{R}_e/\partial\boldsymbol{u}_e$ and derivative arrays $\partial\boldsymbol{R}_e/\partial\boldsymbol{x}_e$, $\partial F_e/\partial\boldsymbol{x}_e$ within the finite element mesh, and forms the global system-level matrices and vectors for the solution of physics and adjoint-sensitivity analysis. The assembly is described as

$$\begin{aligned}
\boldsymbol{R} &\longleftarrow \sum \boldsymbol{R}_e \\
F &\longleftarrow \sum F_e \\
\partial\boldsymbol{R}/\partial\boldsymbol{u} &\longleftarrow \sum \partial\boldsymbol{R}_e/\partial\boldsymbol{u}_e \\
\partial\boldsymbol{R}/\partial\boldsymbol{x} &\longleftarrow \sum \partial\boldsymbol{R}_e/\partial\boldsymbol{x}_e \\
\partial\boldsymbol{F}/\partial\boldsymbol{u} &\longleftarrow \sum \partial\boldsymbol{F}_e/\partial\boldsymbol{u}_e \\
\partial\boldsymbol{F}/\partial\boldsymbol{x} &\longleftarrow \sum \partial\boldsymbol{F}_e/\partial\boldsymbol{x}_e.
\end{aligned} \tag{33}$$

The `Assembler` class also coordinates the parallel, inter-processor communications, and provides options for the ordering of global degrees of freedom.

3) A `Time Integrator` class uses an instance of the `Assembler` and implements the implicit temporal discretization in conjunction with the Newton–Raphson method.

The `Element` and `Function` classes within the deterministic finite element library are illustrated schematically in Figure 5.

B. Stochastic Galerkin Finite Element Frameworks for Physics and Adjoint Sensitivity Analysis

For supporting calculations in the probabilistic domain, consider the implementation of a `Probabilistic Domain` class that stores the probabilistic variables, evaluates the orthonormal basis functions, and supplies the quadrature nodes and weights based on the distribution type. This class abstracts the different options for basis formation (e.g., tensor or complete polynomials) and quadrature setup (e.g., tensor or sparse). If the probabilistic domain discretization is performed first followed by spatial and temporal discretizations, the process would resemble the intrusive SGM illustrated in Figure 2, and as a consequence there will be nothing to place under a layer of probabilistic sampling. Instead, we create a semi-intrusive approach by performing the discretization in a different order to facilitate the reuse of the deterministic implementation. This could take different pathways based on the placement of the probabilistic sampling either before spatial assembly of element block matrices and vectors or after spatial assembly around the global matrices and vectors.

1. Architecture for Probabilistic Sampling Before Spatial Assembly

In Architecture-I, a `Stochastic Element` class implements the `Element` interface, and also stores a deterministic instance of the `Element` class, as shown in Figure 5a. By virtue of this architecture:

1) The `Stochastic Element` class implements the probabilistic sampling of the underlying deterministic capabilities to form N times larger blocks of the stochastic residuals, Jacobians, and adjoint derivative contributions by reusing the instance of the deterministic `Element` it holds through the *composition* (red lines).

2) The `Stochastic Element` is also an element through the *inheritance* of the parent interface (blue lines), and follows through the established pipeline of the assembly, linear algebra, and time-marching algorithms provided by the surrounding `Assembler` and `Time Integrator` without modifications.

Similarly, for the evaluation of the statistical measures and their derivatives, a `Stochastic Function` class implements the `Function` interface and uses a deterministic `Function` instance for sampling, as shown in Figure 5b. The `Stochastic Function` class can be specialized further to evaluate the expectation and variance.

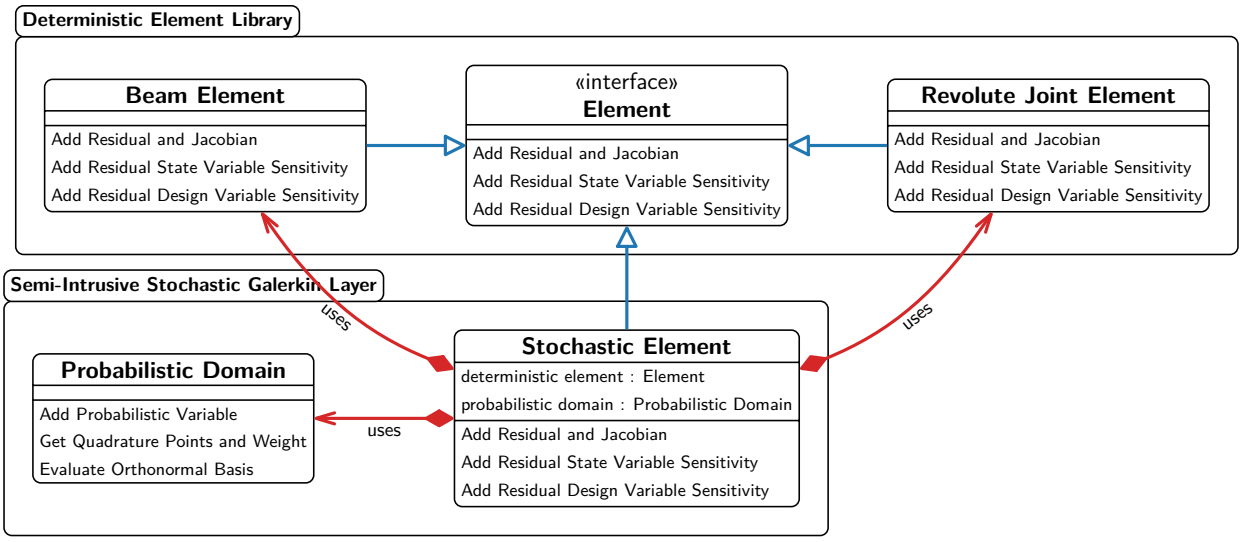

(a) Deterministic and Stochastic Elements

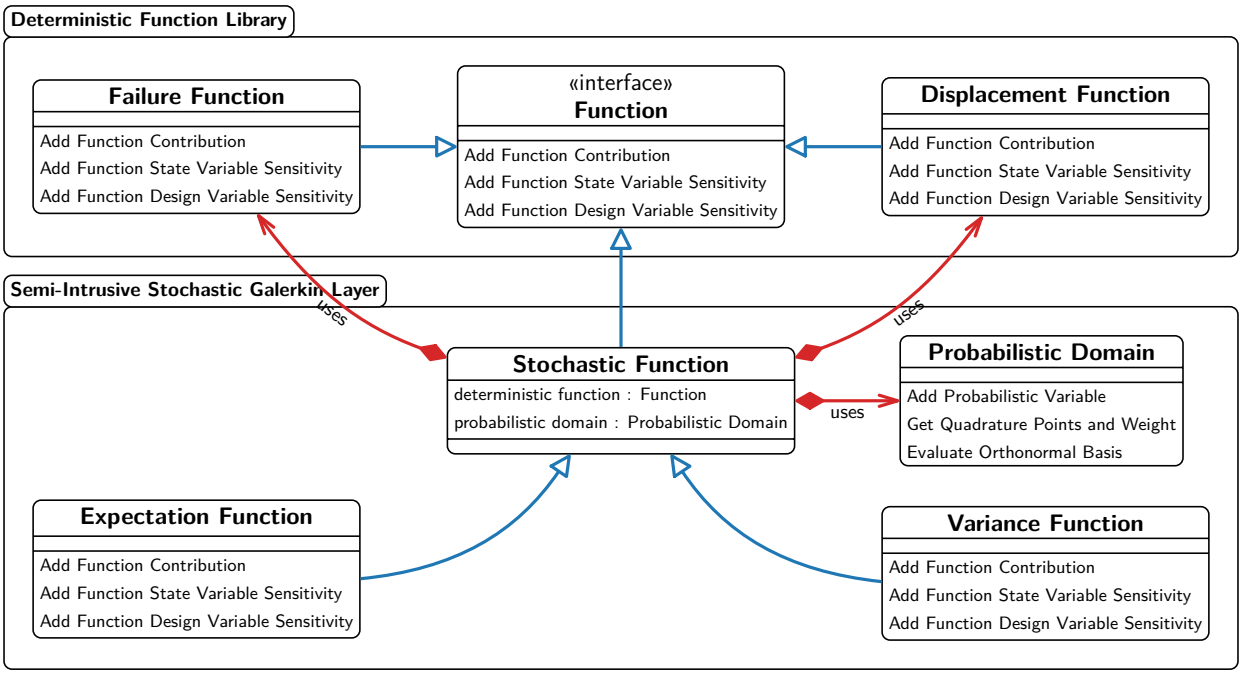

(b) Deterministic and Stochastic Functions

Fig. 5 An architecture showing the stochastic implementation of `Element` and `Function` interfaces. The blue lines denote inheritance and the red lines denote composition among entities. Since the stochastic implementations follow the same interface utilized for deterministic implementations, the assembly and time integration infrastructure of the deterministic framework can be used for the stochastic framework without any modifications.

2. Architecture for Probabilistic Sampling After Spatial Assembly

Alternatively, the probabilistic sampling can be applied surrounding the spatial assembly by implementing a new `Stochastic Assembler` class that implements the `Assembler` interface and uses an instance of the deterministic `Assembler` for the reevaluation of deterministic global matrices and vectors for each quadrature point provided by

the `Probabilistic Domain` class. This architecture is useful when the deterministic framework constraints allow sampling only at the globally assembled system level. The SGM Architecture-I and SGM Architecture-II can differ in the arrangement and ordering of the degrees of freedom (spatial, temporal, and probabilistic), parallel partitioning, and other implementation details, but provide numerically equivalent methods to implement SGM. Architecture-I offers the potential for localized and selective element-level evaluation of contributions to the stochastic Galerkin matrices and vectors, which can be beneficial for speed. For example, if only a group of elements are dependent on random inputs, their block matrices and vectors may be selectively sampled and the other remaining elements may not be reevaluated for each quadrature point.

C. Implementation of SSP and SSM

The classes described above can be tailored to implement the SSP [19, 20] and the SSM discussed in Figure 2 which are classically non-intrusive UQ methods. The SSP can be implemented by invoking the deterministic solution methods contained in the `Assembler` to produce the outputs that are then scaled with basis functions and weights provided at the quadrature points provided by the `Probabilistic Domain`, for each spectral mode decomposition (see Figure 2). The SGM Architecture-II and SSP are subtly different: the former uses deterministic `Assembler` only for the formation of the coupled stochastic system of coefficients, and solves the larger system once using solver methods implemented in `Stochastic Assembler`, whereas the latter uses the deterministic `Assembler` for repeated solutions for each sample point. The SSM can be implemented by simply excluding the weighing contributions of the probabilistic basis functions of SSP implementation, as we are not interested in spectral decomposition in this context.

V. Stochastic Finite Element Analysis and Optimization Under Uncertainty

In this section, we apply our semi-intrusive stochastic Galerkin method on time-dependent finite element problems to verify the accuracy of physics and sensitivity analysis followed by OUU applications. To verify the SGM statistics we use the SSM statistics as the benchmark [34]. To verify the adjoint gradients, we employ the complex-step method to obtain reliable numerical approximations close to machine precision [42]. For these investigations, the SGM Architecture-I and the SSM are implemented utilizing the TACS finite element and adjoint framework.

A. Four-Bar Mechanism

A nonlinear time-dependent four-bar mechanism [59] used for the verification of flexible multibody analysis frameworks is shown in Figure 6. The mechanism contains three flexible bars modeled as Timoshenko beams, three revolute joints (B, C, and D) and an actuator (A) driving the mechanism at a rate of 0.6 rad/s. A rigid fourth-bar is imagined to exist in the mechanism between A and D. The sectional properties of the flexible bars are calculated based on the rectangular cross-sections shown in Figure 6. The bars have an elastic modulus of 207 GPa, density of

7800 kg/m^3, Poisson's ratio of 0.3, and shear correction factor of $5/6$. The revolute axes of the actuator, as well as the joints B and D, are exactly perpendicular to the horizontal plane of the mechanism, whereas the revolute axis of joint C is assumed misaligned by an angle $\theta = \theta(y)$ where $y \sim \mathcal{N}(\mu = 5^\circ, \sigma = 2.5^\circ)$. The deterministic finite element implementation is reused in a black-box fashion for the implementation of SGM, following the semi-intrusive method discussed in Section III.

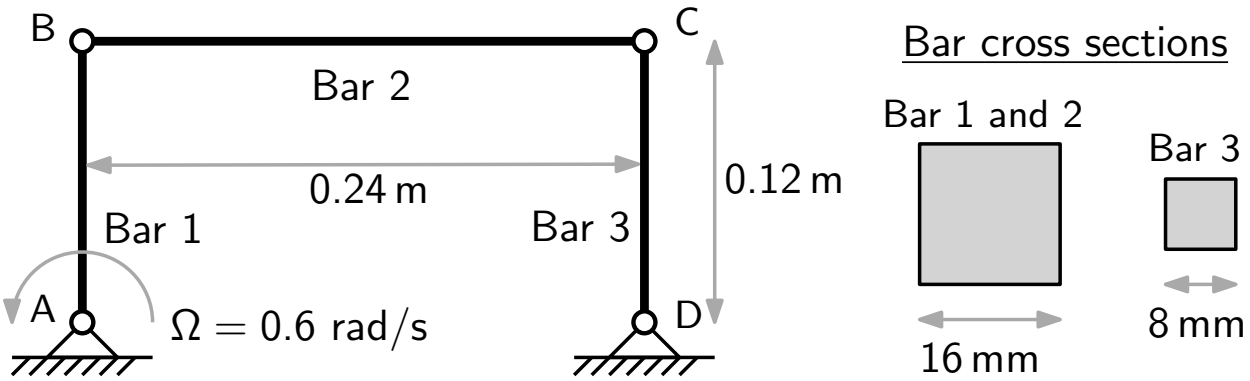

Fig. 6 The schematic of four-bar mechanism (left) and the cross-sectional geometry (right).

1. Verification of Statistics

Figure 7 plots the time history of the mean and variance of the axial force at the mid-point of bar 1. These statistical measures are computed using the semi-intrusive SGM with $N = 3$, 5, and 7 terms in the orthonormal basis set; and the SSM with 15 quadrature points. In one full cycle between $t = 0$ to $t = 12$ s, the axial force exhibits two peaks. The peak occurring between $t = 7.6$ s and $t = 8.1$ s is plotted separately in Figure 7, as well as quantitatively listed in Table 3 along with the deterministic case pertaining to a constant 5° misalignment. The effect of uncertainties on the dynamic response of the mechanism is noticeable in the form of approximately 15% higher peak axial force in bar 1 compared to the deterministic finite element analysis. The results show good agreement of the SGM moments with the SSM statistics for this non-linear case.

Table 3 The statistical measures of the axial force of bar 1 at its mid-point evaluated using SGM and SSM.

Peak Axial-Force	Expectation	Variance
Deterministic	0.5955764	–
SGM (N=3)	0.6870459	0.2585949
SGM (N=5)	0.6858359	0.2625304
SGM (N=7)	0.6866675	0.2614760
SSM (Q=15)	0.6879982	0.2597545

Figure 8 shows the average time taken per time-step for SSM with $Q = 20$ and SGM with $N = 3, 5$ and 7. We scale

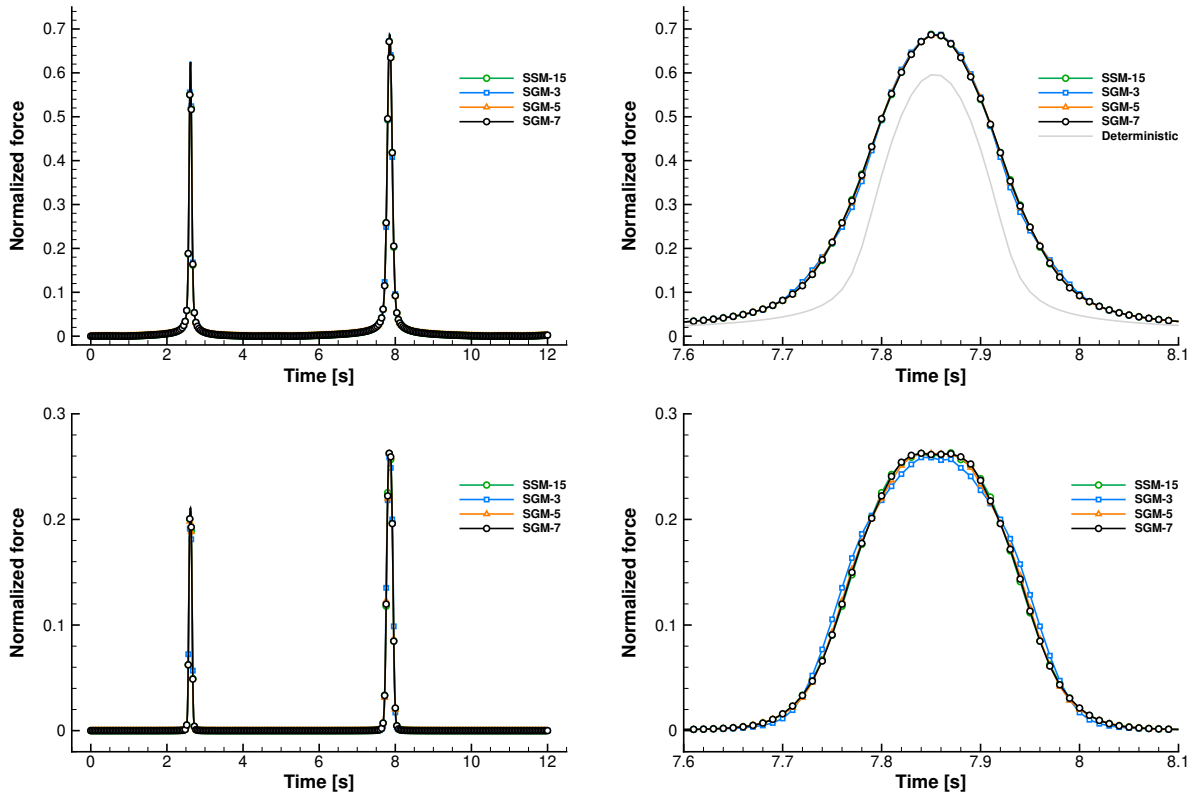

Fig. 7 The mean (top) and variance (bottom) of the normalized axial force in bar AB as a function of time computed using SGM and SSM.

the number of finite element mesh nodes of the Timoshenko beams and plot the computational time with the number of deterministic degrees of freedom. As it can be seen, the SSM is faster for smaller finite element meshes, but its scalability varies as the mesh size increases. The SGM maintains an almost linear scaling with the degrees of freedom. For this case setup, the computational time of SGM ($N = 3$) is comparable to the SSM. However, note that Q and N are tunable parameters and this study may not be indicative of higher dimensional scaling when there are more random variables.

2. Verification of Adjoint Derivatives

The stochastic adjoint gradient verification is performed for three structural output functions: the mass, the maximum out-of-plane displacement, and the maximum axial stress based failure using the uniform width of bars AB and BC as the design variable. The maximum displacement and failure response are estimated using Eq. (7) with $\rho_{ks} = 10^4$. Table 4 lists the gradients of the expectation and variance of these functions, evaluated using the stochastic-adjoint method outlined in Section III.C and the complex-step derivative estimate. The gradients are observed to exhibit sufficient accuracy for solving the OUU problems using gradient-based methods.

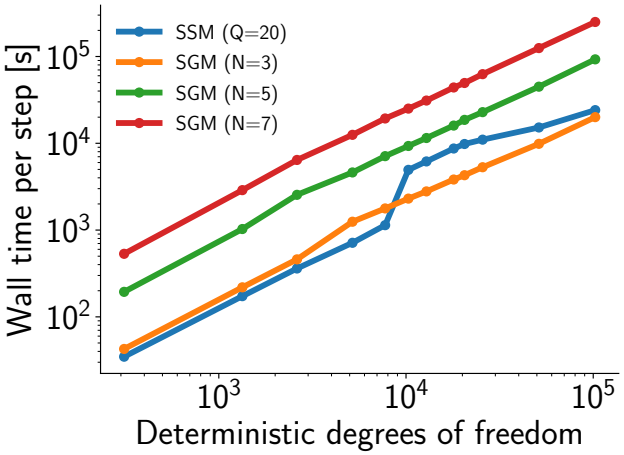

Fig. 8 The averaged wall time for each time-step taken by the SSM and SGM with the number of deterministic degrees of freedom (P) in the model.

Table 4 Derivatives with respect to the width of bars AB and BC evaluated using the complex-step method with step size 10^{-30} and the stochastic Galerkin adjoint method.

Function	Complex-Step Gradient	Adjoint Gradient	Relative Error
mass	1078.27**2000000680**	1078.27**1999999841**	7.78×10^{-13}
expectation of displacement	49.023**65922158757**	49.023**04466365254**	1.25×10^{-5}
variance of displacement	70.22**008165947029**	70.22**135562360499**	1.81×10^{-5}
expectation of failure	-0.10678349**91432143**	-0.10678344**43529120**	5.13×10^{-7}
variance of failure	-1.57732**7462264513** $\times 10^{-4}$	-1.57732**8512903997** $\times 10^{-4}$	6.66×10^{-5}

3. Optimization Under Uncertainty

Next, we formulate an OUU problem with the four-bar model as follows

$$
\begin{aligned}
\text{minimize} \quad & f(\boldsymbol{x}) \triangleq \mathbb{E}[\text{mass}] \\
\text{subject to} \quad & c_1(\boldsymbol{x}) \triangleq \mathbb{E}[\text{failure}] + K \cdot \mathbb{S}[\text{failure}] \leq 1.0 \\
& c_2(\boldsymbol{x}) \triangleq \mathbb{E}[\text{displacement}] + K \cdot \mathbb{S}[\text{displacement}] \leq 5\,\text{mm} \\
\text{bounds} \quad & 5\,\text{mm} \leq \text{widths} \leq 25\,\text{mm}.
\end{aligned}
$$

The mass objective refers to the overall mass of the mechanism, the displacement constraint refers to the displacement component that is out of the plane, and the failure is evaluated based on allowed normal (axial) force in the bars. We use spatio-temporal aggregation of constraint functions based on KS formulation [54, 55] for displacement and failure. We perform five optimization runs composed of one deterministic and four probabilistic OUU runs with $K = 0, 1, 2$ and 3, and compare the designs in Table 5. The widths of the bars AB and BC have a larger impact than the width of the third bar CD, as bar BC encounters the highest magnitude of force and displacement throughout the simulation range. We

Table 5 Four-bar mechanism designs resulting from the deterministic and optimization under uncertainty.

Quantity	Deterministic	$K = 0$	$K = 1$	$K = 2$	$K = 3$
width AB & BC	5.0	5.0	13.0	18.3	23.5
width CD	5.0	5.0	5.0	6.0	7.0
mass [kg]	1.1	1.1	6.02	11.7	19.3
failure [% max]	47%	55	90	100	100
displacement [% max]	78.22	78.72	100	100	100

notice that the optimizer adds width to the beams as we incorporate more constraint satisfaction through the parameter K.

B. Flexible Remote Manipulator System

Next, the semi-intrusive stochastic Galerkin framework is applied to a probabilistic design optimization problem under uncertainty, based on the dynamics of a robotic manipulator arm. Robotic arms like the Canadarm and Dextre are utilized in space missions for tasks such as moving payloads, assembling space systems, assisting with docking, and conducting maintenance activities [60].

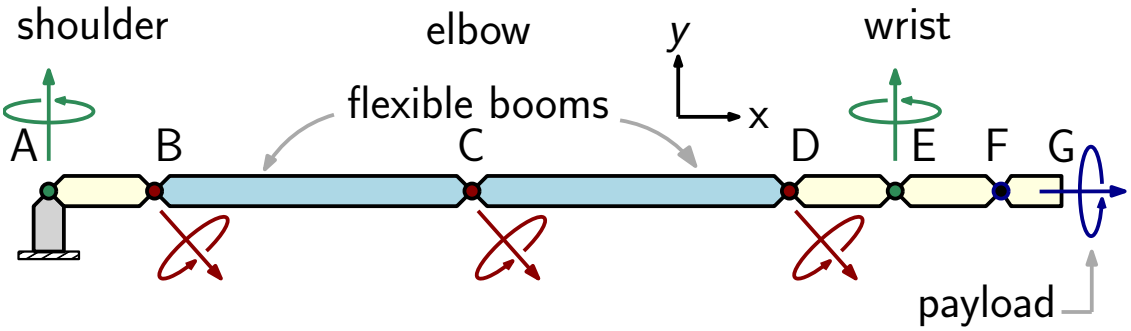

Fig. 9 A schematic of the remote manipulator model with six joint degrees of freedom.

1. Setup of the Finite Element Analysis

We utilize a simplified robotic manipulator system [61–66] depicted in Figure 9 as our model. This model, similar in function to a human arm, features six joint degrees of freedom. The model has two revolute joints at the shoulder, one at the elbow between the flexible booms BC and CD, and three more near the wrist. The joints at A and E allow yawing motion about the $y-$axis; the joints at B, C and D allow pitching motion about the $z-$axis; and the joint at F allows rolling motion about the $x-$axis. The material properties of the booms are: Young's modulus of 207 GPa, density of 7800 kg/m^3, Poisson's ratio of 0.3, shear correction factor of $5/6$. The lengths $AB = 0.9$ m, $BC = 6.4$ m, $CD = 7.0$ m, $DE = 0.5$ m, $EF = 0.8$ m and $FG = 0.6$ m. The masses of the rigid bodies are: $m_1 = 95$ kg, $m_4 = 8$ kg, $m_5 = 44$ kg, $m_6 = 41$ kg. The two longer booms BC and CD are modeled as flexible Timoshenko beams of square cross-sections 25 cm wide.

The control inputs are assumed to maintain the revolute joints at rates: $\omega_A = \omega_B = \omega_C = \omega_D = \omega_E = \omega_F = 0.1$ rad/s. The motion is simulated with these parameters and the initial configuration as the fully extended arm for a duration $t_f = 5$ s (see Figure 10).

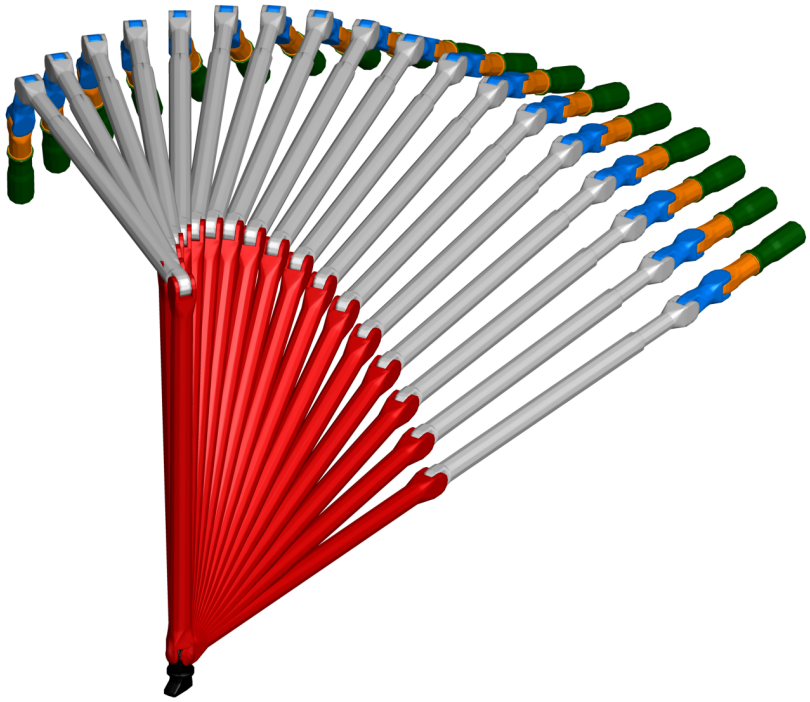

Fig. 10 The time-lapse of the simulated deterministic motion.

2. Optimization Under Uncertain Payloads

The robotic manipulator system needs to be designed for handling a wide range of masses for assembly and maintenance operations on space stations, and we demonstrate the suitability of the OUU concepts in this context. We model the mass of the payload as a function of random variable with Gaussian distribution as $y \sim \mathcal{N}(\mu = 10^5\,\text{kg}, \sigma = 5 \cdot 10^4\,\text{kg})$. The stochastic Galerkin basis set is formed with $N = 3$ orthonormal Hermite polynomials, that yield three probabilistic degrees of freedom to each deterministic degree of freedom in the finite element model. We setup an optimization problem to minimize the mass of the system subject to stress-based failure constraint as follows

$$\begin{aligned} &\text{minimize} && f(\boldsymbol{x}) \triangleq \mathbb{E}[\text{mass}] \\ &\text{subject to} && c(\boldsymbol{x}) \triangleq \mathbb{E}[\text{failure}] + \beta \cdot \mathbb{S}[\text{failure}] \leq 1.0 \\ &\text{bounds} && 25\,\text{mm} \leq \text{widths} \leq 50\,\text{mm}. \end{aligned} \tag{34}$$

The two design variables are the rectangular cross-sectional width of the booms BC and CD. In this problem setup, the mass objective function has no dependence on the random variable since the Gaussian-random payload masses

do not contribute to the mass of the flexible booms. We still evaluate the expectation for verification purposes. The optimization constraint is formulated using the expectation and standard deviation of the aggregated maximum failure in spatio-temporal domains based on the KS aggregation method [54, 55] with $\rho_{ks} = 10^4$. First, a verification of the adjoint derivatives of the statistics is performed using the complex-step method prior to optimization, and the values are listed in Table 6.

Table 6 The complex-step verification of adjoint derivatives for the robotic manipulator system.

Quantity	Mass	Failure
adjoint $d\mathbb{E}[\bar{\mathsf{F}}]/d\boldsymbol{x}$	$1.24800000000001\mathbf{979} \times 10^5$	-3.7659**7889920338691**
complex $d\mathbb{E}[\bar{\mathsf{F}}]/d\boldsymbol{x}$	$1.24800000000001\mathbf{819} \times 10^5$	-3.7659**6706242138746**
relative error	1.3×10^{-15}	3.1×10^{-6}
adjoint $d\mathbb{V}[\bar{\mathsf{F}}]/d\boldsymbol{x}$	–	$-4.4644\mathbf{2271585651973} \times 10^{-1}$
complex $d\mathbb{V}[\bar{\mathsf{F}}]/d\boldsymbol{x}$	–	$-4.4644\mathbf{4953483493667} \times 10^{-1}$
relative error	–	6.0×10^{-6}

The optimization problem (34) is solved for constraint parameter K ranging from zero to seven. For baseline design comparisons, a deterministic optimization problem with a constant payload mass of 100, 000 kg is also solved. The results from the nine optimization runs are tabulated in Table 7. It can be seen that the widths increase as we require more constraint satisfaction through the parameter K. For example, the design pertaining to $K = 6$ is six standard deviations away from the expected failure manifold, where a deterministic optimizer would converge. When the constraints become 100% active for the OUU designs ($K = 2$ to $K = 7$), the optimizer adds mass to the structure. Figure 11 provides a visualization of the two-dimensional design space, and plots the trajectory of the *final* optimized designs $\boldsymbol{x}(K)$ as K increases from zero to seven.

Table 7 The optimized designs of the robotic manipulator arm produced from deterministic optimization and OUU.

Quantity	Deterministic	$K = 0$	$K = 1$	$K = 2$	$K = 3$	$K = 4$	$K = 5$	$K = 6$	$K = 7$
x_1 [cm] – bar BC	25.00	25.00	25.00	27.17	30.3	34.3	38.5	42.8	47.1
x_2 [cm] – bar CD	25.00	25.00	25.00	25.00	25.0	27.8	31.1	34.7	38.1
$\mathbb{E}$[constraint]	–	0.729	0.729	0.650	0.552	0.482	0.431	0.388	0.353
$\mathbb{S}$[constraint]	–	0.196	0.196	0.175	0.149	0.129	0.114	0.102	0.092
constraint activity %	76.8	72.9	92.5	100	100	100	100	100	100
optimizer iterations	7	7	7	9	8	34	62	43	41
elapsed time [min]	0.20	5.35	4.48	6.02	3.71	12.08	35.20	19.28	27.84

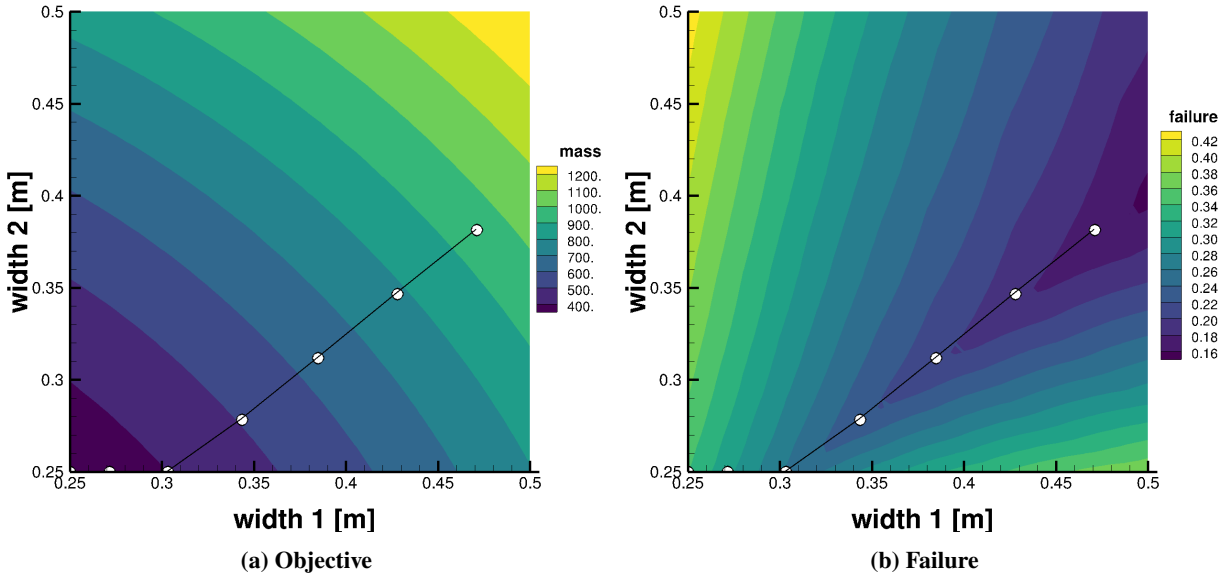

(a) Objective **(b) Failure**

Fig. 11 Visualization of optimization design space with contours of the mass and failure alongside the optimal OUU designs.

VI. Conclusion

In this paper, we presented a formulation of the stochastic Galerkin method that uses the stochastic sampling of an underlying deterministic finite element framework. The proposed sampling-based semi-intrusive SGM leverages a deterministic finite-element framework to create a stochastic finite-element framework for OUU that includes adjoint-sensitivity analysis. The method is semi-intrusive since its implementation reuses the underlying deterministic framework. The software architectures implementing the SGM at the global-system and the local-element scales were discussed, within a generalized stochastic framework where other uncertainty propagation methods like the SSP and the SSM can also be implemented. For verification, the statistics computed using the SGM were compared to the statistics computed using the SSM on nonlinear time-dependent finite element problems. A stochastic adjoint formulation was presented and numerically verified using the complex-step method. The computational framework for stochastic Galerkin finite element analysis and adjoint-sensitivity analysis was utilized to solve OUU problems based on flexible multibody dynamics.

References

[1] Hirsch, C., Wunsch, D., Szumbarski, J., Łaniewski-Wołłk, Ł., and Pons-Prats, J. (eds.), *Uncertainty Management for Robust Industrial Design in Aeronautics*, Springer International Publishing, 2019. https://doi.org/10.1007/978-3-319-77767-2.

[2] Kumar, D., Raisee, M., and Lacor, C., *Combination of Polynomial Chaos with Adjoint Formulations for Optimization Under Uncertainties*, Springer International Publishing, Cham, 2019, pp. 567–582. https://doi.org/10.1007/978-3-319-77767-2_35, URL https://doi.org/10.1007/978-3-319-77767-2_35.

[3] Sahinidis, N. V., "Optimization under uncertainty: state-of-the-art and opportunities," *Computers & Chemical Engineering*, Vol. 28, No. 6, 2004, pp. 971–983. https://doi.org/https://doi.org/10.1016/j.compchemeng.2003.09.017, URL https://www.sciencedirect.com/science/article/pii/S0098135403002369, FOCAPO 2003 Special issue.

[4] Giunta, A., Eldred, M., Swiler, L., Trucano, T., and Wojtkiewicz, S., "Perspectives in Optimization Under Uncertainty: Algorithms and Applications," *10th AIAA/ISSMO Multidisciplinary Analysis and Optimization Conference*, 2004. https://doi.org/10.2514/6.2004-4451, URL https://doi.org/10.2514/6.2004-4451, AIAA 2004-4451.

[5] Ng, L. W.-T., Huynh, D. B. P., and Willcox, K., "Multifidelity Uncertainty Propagation for Optimization Under Uncertainty," *12th AIAA Aviation Technology, Integration, and Operations (ATIO) Conference and 14th AIAA/ISSMO Multidisciplinary Analysis and Optimization Conference*, 2012. https://doi.org/10.2514/6.2012-5602, URL https://doi.org/10.2514/6.2012-5602, AIAA 2012-5602.

[6] Eldred, M., Giunta, A., Wojtkiewicz, S., and Trucano, T., "Formulations for Surrogate-Based Optimization Under Uncertainty," *9th AIAA/ISSMO Symposium on Multidisciplinary Analysis and Optimization*, 2002. https://doi.org/10.2514/6.2002-5585, URL https://doi.org/10.2514/6.2002-5585, AIAA 2002-5585.

[7] Tiesler, H., Kirby, R. M., Xiu, D., and Preusser, T., "Stochastic Collocation for Optimal Control Problems with Stochastic PDE Constraints," *SIAM Journal on Control and Optimization*, Vol. 50, No. 5, 2012, pp. 2659–2682. https://doi.org/10.1137/110835438, URL https://doi.org/10.1137/110835438.

[8] Keshavarzzadeh, V., Fernandez, F., and Tortorelli, D. A., "Topology optimization under uncertainty via non-intrusive polynomial chaos expansion," *Computer Methods in Applied Mechanics and Engineering*, Vol. 318, 2017, pp. 120 – 147. https://doi.org/10.1016/j.cma.2017.01.019.

[9] Slotnick, J., Khodadoust, A., Alonso, J., Darmofal, D., Gropp, W., Lurie, E., and Mavriplis, D., "CFD Vision 2030 Study: A Path to Revolutionary Computational Aerosciences," Tech. Rep. NASA/CR–2014-218178, NASA Langley Research Center, 2014.

[10] Geiersbach, C., and Wollner, W., "A Stochastic Gradient Method With Mesh Refinement for PDE-Constrained Optimization Under Uncertainty," *SIAM Journal on Scientific Computing*, Vol. 42, No. 5, 2020, pp. A2750–A2772. https://doi.org/10.1137/19M1263297, URL https://doi.org/10.1137/19M1263297.

[11] Eldred, M., Webster, C., and Constantine, P., "Evaluation of Non-Intrusive Approaches for Wiener-Askey Generalized Polynomial Chaos," *49th AIAA/ASME/ASCE/AHS/ASC Structures, Structural Dynamics, and Materials Conference, 16th AIAA/ASME/AHS Adaptive Structures Conference,10th AIAA Non-Deterministic Approaches Conference, 9th AIAA Gossamer Spacecraft Forum, 4th AIAA Multidisciplinary Design Optimization Specialists Conference*, 2008. https://doi.org/10.2514/6.2008-1892, URL https://doi.org/10.2514/6.2008-1892, AIAA 2008-1892.

[12] Jones, B. A., Doostan, A., and Born, G. H., "Nonlinear Propagation of Orbit Uncertainty Using Non-Intrusive Polynomial

Chaos," *Journal of Guidance, Control, and Dynamics*, Vol. 36, No. 2, 2013, pp. 430–444. https://doi.org/10.2514/1.57599, URL https://doi.org/10.2514/1.57599.

[13] Peherstorfer, B., Gunzburger, M., and Willcox, K., "Convergence analysis of multifidelity Monte Carlo estimation," *Numerische Mathematik*, Vol. 139, 2018, pp. 1–25. https://doi.org/10.1007/s00211-018-0945-7.

[14] Eldred, M., "Recent Advances in Non-Intrusive Polynomial Chaos and Stochastic Collocation Methods for Uncertainty Analysis and Design," *50th AIAA/ASME/ASCE/AHS/ASC Structures, Structural Dynamics, and Materials Conference*, 2009. https://doi.org/10.2514/6.2009-2274, URL https://doi.org/10.2514/6.2009-2274, AIAA 2009-2274.

[15] Cheng, H., and Sandu, A., "Collocation Least-Squares Polynomial Chaos Method," *Proceedings of the 2010 Spring Simulation Multiconference*, Society for Computer Simulation International, San Diego, CA, USA, 2010. https://doi.org/10.1145/1878537.1878621, URL https://doi.org/10.1145/1878537.1878621.

[16] Xiu, D., "Fast Numerical Methods for Stochastic Computations: A Review," *Communications in Computational Physics*, Vol. 5, No. 2-4, 2009, pp. 242–272. URL http://global-sci.org/intro/article_detail/cicp/7732.html.

[17] Gunzburger, M., G. Webster, C., and Zhang, G., *Handbook of Uncertainty Quantification*, Springer Cham, 2017, Chap. Sparse Collocation Methods for Stochastic Interpolation and Quadrature, pp. 717–762. https://doi.org/10.1007/978-3-319-12385-1_29.

[18] Gunzburger, M., "An Applied/Computational Mathematician's View of Uncertainty Quantification for Complex Systems," *Proceedings of 2015 and 2016 ACMES Conferences*, 2019, pp. 133–151. https://doi.org/10.1007/978-1-4939-9051-1_5.

[19] Reagan, M., Najm, H., Ghanem, R., and Knio, O., "Uncertainty quantification in reacting-flow simulations through non-intrusive spectral projection," *Combustion and Flame*, Vol. 132, 2003, pp. 545–555. https://doi.org/10.1016/S0010-2180(02)00503-5.

[20] Acharjee, S., and Zabaras, N., "A non-intrusive stochastic Galerkin approach for modeling uncertainty propagation in deformation processes," *Computers & Structures*, Vol. 85, No. 5, 2007, pp. 244–254. https://doi.org/10.1016/j.compstruc.2006.10.004.

[21] Maître, O. P. L., and Knio, O. M., *Spectral Methods for Uncertainty Quantification, Scientific Computation*, Springer, 2010. https://doi.org/10.1007/978-90-481-3520-2.

[22] Ernst, O., and Ullmann, E., "Stochastic Galerkin Matrices," *SIAM Journal on Matrix Analysis and Applications*, Vol. 31, No. 4, 2010, pp. 1848–1872. https://doi.org/10.1137/080742282.

[23] Delgado, P., and Kumar, V., "A stochastic Galerkin approach to uncertainty quantification in poroelastic media," *Applied Mathematics and Computation*, Vol. 266, 2015, pp. 328–338. https://doi.org/10.1016/j.amc.2015.04.127.

[24] Walters, R., "Towards Stochastic Fluid Mechanics via Polynomial Chaos," *41st Aerospace Sciences Meeting and Exhibit*, 2003. https://doi.org/10.2514/6.2003-413, AIAA 2003-413.

[25] Xiu, D., and Karniadakis, G., "The Wiener–Askey Polynomial Chaos for Stochastic Differential Equations," *SIAM Journal on Scientific Computing*, Vol. 24, No. 2, 2002, pp. 619–644. https://doi.org/10.1137/S1064827501387826.

[26] Ghanem, R., and Red-Horse, J., "Propagation of probabilistic uncertainty in complex physical systems using a stochastic finite element approach," *Physica D: Nonlinear Phenomena*, Vol. 133, No. 1, 1999, pp. 137–144. https://doi.org/10.1016/S0167-2789(99)00102-5, URL https://www.sciencedirect.com/science/article/pii/S0167278999001025.

[27] Ghanem, R., and Spanos, P. D., *Stochastic Finite Elements: A Spectral Approach (2nd edition)*, New York: Springer, 1991. https://doi.org/10.1007/978-1-4612-3094-6.

[28] Ghanem, R., "Ingredients for a general purpose stochastic finite elements implementation," *Computer Methods in Applied Mechanics and Engineering*, Vol. 168, No. 1, 1999, pp. 19 – 34. https://doi.org/10.1016/S0045-7825(98)00106-6.

[29] Gutiérrez, M. A., and Krenk, S., *Stochastic Finite Element Methods*, John Wiley & Sons, 2004, Chap. 20. https://doi.org/10.1002/0470091355.ecm044.

[30] Matthies, H. G., *Uncertainty Quantification with Stochastic Finite Elements*, John Wiley & Sons, 2007, Chap. 27. https://doi.org/10.1002/0470091355.ecm071.

[31] D. Gunzburger, M., G. Webster, C., and Zhang, G., "Stochastic finite element methods for partial differential equations with random input data," *Acta Numerica*, Vol. 23, 2014, pp. 521–650. https://doi.org/10.1017/S0962492914000075.

[32] Abgrall, R., and Tokareva, S., "The Stochastic Finite Volume Method," *SEMA SIMAI Springer Series*, 2017, pp. 1–57. https://doi.org/10.1007/978-3-319-67110-9_1.

[33] Babuska, I., Tempone, R., and Zouraris, G. E., "Galerkin Finite Element Approximations of Stochastic Elliptic Partial Differential Equations," *SIAM Journal on Numerical Analysis*, Vol. 42, No. 2, 2004, pp. 800–825. https://doi.org/10.1137/S0036142902418680, URL https://doi.org/10.1137/S0036142902418680.

[34] Bäck, J., Nobile, F., Tamellini, L., and Tempone, R., "Stochastic Spectral Galerkin and Collocation Methods for PDEs with Random Coefficients: A Numerical Comparison," *Spectral and High Order Methods for Partial Differential Equations*, edited by J. S. Hesthaven and E. M. Rønquist, Springer Berlin Heidelberg, Berlin, Heidelberg, 2011, pp. 43–62.

[35] Wang, B., Orndorff, N. C., and Hwang, J. T., *Optimally tensor-structured quadrature rule for uncertainty quantification*, 2023. https://doi.org/10.2514/6.2023-0741, URL https://arc.aiaa.org/doi/abs/10.2514/6.2023-0741.

[36] Roderick, O., Anitescu, M., and Fischer, P., "Polynomial Regression Approaches Using Derivative Information for Uncertainty Quantification," *Nuclear Science and Engineering*, Vol. 164, No. 2, 2010, pp. 122–139. https://doi.org/10.13182/NSE08-79, URL https://doi.org/10.13182/NSE08-79.

[37] Li, Y., Anitescu, M., Roderick, O., and Hickernell, F., "Orthogonal Bases for Polynomial Regression with Derivative Information in Uncertainty Quantification," *International Journal for Uncertainty Quantification*, Vol. 1, No.4, 2011, pp. 297–320. https://doi.org/10.1615/Int.J.UncertaintyQuantification.2011002790.

[38] Han, Z. H., Goertz, S., and Zimmermann, R., "Improving variable-fidelity surrogate modeling via gradient-enhanced kriging and a generalized hybrid bridge function," *Aerospace Science and Technology*, 2012. https://doi.org/10.1016/j.ast.2012.01.006.

[39] Boopathy, K., Rumpfkeil, M. P., and Kolonay, R. M., *Robust Optimization of a Wing Under Structural and Material Uncertainties*, 2015. https://doi.org/10.2514/6.2015-0920, URL https://arc.aiaa.org/doi/abs/10.2514/6.2015-0920.

[40] Boopathy, K., and Rumpfkeil, M. P., "Unified Framework for Training Point Selection and Error Estimation for Surrogate Models," *AIAA Journal*, Vol. 53, 2014, pp. 215–234. https://doi.org/10.2514/1.J053064.

[41] Boopathy, K., and Rumpfkeil, M. P., *Robust Optimizations of Structural and Aerodynamic Designs*, 2014. https://doi.org/10.2514/6.2014-2595, URL https://arc.aiaa.org/doi/abs/10.2514/6.2014-2595.

[42] Martins, J. R. R. A., Alonso, J. J., and Reuther, J. J., "A Coupled-Adjoint Sensitivity Analysis Method for High-Fidelity Aero-Structural Design," *Optimization and Engineering*, Vol. 6, No. 1, 2005, pp. 33–62. https://doi.org/10.1023/B:OPTE.0000048536.47956.62.

[43] Le Maıtre, O. P., Knio, O. M., Najm, H. N., and Ghanem, R. G., "A Stochastic Projection Method for Fluid Flow: I. Basic Formulation," *Journal of Computational Physics*, Vol. 173, No. 2, 2001, pp. 481–511. https://doi.org/https://doi.org/10.1006/jcph.2001.6889, URL https://www.sciencedirect.com/science/article/pii/S0021999101968895.

[44] Wang, G., and Liao, Q., "Reduced basis stochastic Galerkin methods for partial differential equations with random inputs," *Applied Mathematics and Computation*, Vol. 463, 2024, p. 128375. https://doi.org/https://doi.org/10.1016/j.amc.2023.128375, URL https://www.sciencedirect.com/science/article/pii/S0096300323005441.

[45] Matthies, H. G., and Keese, A., "Galerkin methods for linear and nonlinear elliptic stochastic partial differential equations," *Computer Methods in Applied Mechanics and Engineering*, Vol. 194, No. 12, 2005, pp. 1295–1331. https://doi.org/https://doi.org/10.1016/j.cma.2004.05.027, URL https://www.sciencedirect.com/science/article/pii/S0045782504003950, special Issue on Computational Methods in Stochastic Mechanics and Reliability Analysis.

[46] Ullmann, E., "A Kronecker Product Preconditioner for Stochastic Galerkin Finite Element Discretizations," *SIAM Journal on Scientific Computing*, Vol. 32, No. 2, 2010, pp. 923–946. https://doi.org/10.1137/080742853, URL https://doi.org/10.1137/080742853.

[47] Gaignaire, R., Guyomarc'h, F., Moreau, O., Clenet, S., and Sudret, B., "Speeding Up SSFEM Computation Using Kronecker Tensor Products," *IEEE Transactions on Magnetics*, Vol. 45, No. 3, 2009, pp. 1432–1435. https://doi.org/10.1109/TMAG.2009.2012662.

[48] Sharma, S., Jolivet, P., Dolean, V., and Sarkar, A., "Multilevel Scalable Solvers for Stochastic Linear and Nonlinear Problems," *arXiv e-prints*, 2023, arXiv:2310.14649. https://doi.org/10.48550/arXiv.2310.14649.

[49] Subber, W., and Sarkar, A., "A domain decomposition method of stochastic PDEs: An iterative solution techniques using a two-level scalable preconditioner," *Journal of Computational Physics*, Vol. 257, 2014, pp. 298–317. https://doi.org/https://doi.org/10.1016/j.jcp.2013.08.058, URL https://www.sciencedirect.com/science/article/pii/S0021999113006025.

[50] Boopathy, K., "Adjoint Based Design Optimization of Systems with Time Dependent Physics and Probabilistically Modeled Uncertainties," Ph.D. thesis, Georgia Institute of Technology, Atlanta, GA, 2020. URL {http://hdl.handle.net/1853/63658}.

[51] Boopathy, K., and Kennedy, G., "Semi-Intrusive Uncertainty Propagation and Adjoint Sensitivity Analysis Using the Stochastic Galerkin Method," *AIAA Scitech 2020 Forum*, 2020. https://doi.org/10.2514/6.2020-1146, AIAA 2020-1146.

[52] Chatzimanolakis, M., Kantarakias, K.-D., Asouti, V., and Giannakoglou, K., "A painless intrusive polynomial chaos method with RANS-based applications," *Computer Methods in Applied Mechanics and Engineering*, Vol. 348, 2019, pp. 207 – 221. https://doi.org/10.1016/j.cma.2019.01.018.

[53] Bauchau, O. A., *Flexible Multibody Dynamics*, Springer Netherlands, 2011. https://doi.org/10.1007/978-94-007-0335-3.

[54] Kreisselmeier, G., and Steinhauser, R., "Systematic control design by optimizing a vector performance index," *International Federation of Active Controls Symposium on Computer-Aided Design of Control Systems*, Zurich, Switzerland, 1979.

[55] Kennedy, G. J., and Hicken, J. E., "Improved constraint-aggregation methods," *Computer Methods in Applied Mechanics and Engineering*, Vol. 289, 2015, pp. 332 – 354. https://doi.org/10.1016/j.cma.2015.02.017.

[56] Boopathy, K., and Kennedy, G. J., "Parallel Finite Element Framework for Rotorcraft Multibody Dynamics and Discrete Adjoint Sensitivities," *AIAA Journal*, Vol. 57, No. 8, 2019, pp. 1–14. https://doi.org/10.2514/1.J056585.

[57] Boopathy, K., and Kennedy, G., "Adjoint-based derivative evaluation methods for flexible multibody systems with rotorcraft applications," *55th AIAA Aerospace Sciences Meeting*, Grapevine, TX, 2017. https://doi.org/10.2514/6.2017-1671, AIAA 2017-1671.

[58] Kennedy, G. J., and Martins, J. R., "A parallel finite-element framework for large-scale gradient-based design optimization of high-performance structures," *Finite Elements in Analysis and Design*, Vol. 87, 2014, pp. 56–73. https://doi.org/10.1016/j.finel.2014.04.011, URL https://www.sciencedirect.com/science/article/pii/S0168874X14000730.

[59] Bauchau, O. A., Betsch, P., Cardona, A., Gerstmayr, J., Jonker, B., Masarati, P., and Sonneville, V., "Validation of flexible multibody dynamics beam formulations using benchmark problems," *Multibody System Dynamics*, Vol. 37, No. 1, 2016, pp. 29–48. https://doi.org/10.1007/s11044-016-9514-y.

[60] Michael Hiltz, K. B., Craig Rice, and Allison, R., "CANADARM: 20 YEARS OF MISSION SUCCESS THROUGH ADAPTATION," 6th International Symposium on Artificial Intelligence and Robotics & Automation in Space, i-SAIRAS, June 18-22, 2001.

[61] Damaren, C., and Sharf, I., "Simulation of Flexible-Link Manipulators With Inertial and Geometric Nonlinearities," *Journal of Dynamic Systems, Measurement, and Control*, Vol. 117, No. 1, 1995, pp. 74–87. https://doi.org/10.1115/1.2798525.

[62] Damaren, C. J., "Passivity analysis for flexible multilink space manipulators," *Journal of Guidance, Control, and Dynamics*, Vol. 18, No. 2, 1995, pp. 272–279. https://doi.org/10.2514/3.21380.

[63] Damaren, C., "Approximate inverse dynamics and passive feedback for flexible manipulators with large payloads," *IEEE Transactions on Robotics and Automation*, Vol. 12, No. 1, 1996, pp. 131–138. https://doi.org/10.1109/70.481758.

[64] Walsh, A., and Forbes, J. R., "Modeling and Control of Flexible Telescoping Manipulators," *IEEE Transactions on Robotics*, Vol. 31, No. 4, 2015, pp. 936–947. https://doi.org/10.1109/TRO.2015.2441473.

[65] Puig, L., Barton, A., and Rando, N., "A review on large deployable structures for astrophysics missions," *Acta Astronautica*, Vol. 67, 2010, pp. 12–26. https://doi.org/10.1016/j.actaastro.2010.02.021.

[66] Llop, J. V., Drew, J., Zappulla, R., and Romano, M., "Autonomous Capture of a Resident Space Object by a Spacecraft with a RoboticManipulator: Analysis, Simulation and Experiments," *AIAA/AAS Astrodynamics Specialist Conference*, 2016. https://doi.org/10.2514/6.2016-5269.